ADVANCED MATERIALS INTERFACES
www.advmatinterfaces.de

Structure, Composition, Transport Properties, and Electrochemical Performance of the Electrode-Electrolyte Interphase in Non-Aqueous Na-Ion Batteries

Miguel Ángel Muñoz-Márquez, Maider Zarrabeitia, Stefano Passerini,* and Teófilo Rojo**

Rechargeable Li-ion battery technology has progressed due to the development of a suitable combination of electroactive materials, binders, electrolytes, additives, and electrochemical cycling protocols that resulted in the formation of a stable electrode-electrolyte interphase. It is expected that Na-ion technology will attain a position comparable to Li-ion batteries dependent on advancements in establishing a stable electrode-electrolyte interphase. However, Li and Na are both alkali metals with similar characteristics, yet the physicochemical properties of these systems differ. For this reason, a detailed study on the electrode-electrolyte interphase properties, composition, and structure is required to understand the factors that influence the battery's behavior. Herein, the research that has been performed on the electrode-electrolyte interphase for both anode and cathode in the most important families of electrode materials, including carbonate ester-based and advanced electrolytes such as ether-based carbonates and ionic liquids is presented.

1. Introduction

The use of rechargeable batteries in our society and their role in the ongoing transition towards a carbon-free energy model is of paramount importance.[1–3] Great research efforts have been made towards the development of new battery materials that increase cycle life, safety, and energy density, as well as power density[4,5] along with investigations focused on understanding novel battery chemistries that can become an alternative to the dominant liquid electrolyte-based Li-ion battery technology.[6–10] Na-ion technologies have emerged as one of the most promising for battery applications.[11–15] Interestingly, while the attention is on a given battery chemistry that promises one order of magnitude increase of the energy density,[16,17] or in a specific electrode material that outperforms currently available electroactive materials in terms of specific capacity or operating voltage,[18–20] there is a tendency to overlook the crucial role that battery interfaces play in the safety, power capability, morphology of lithium deposits, shelf-life, and cycle life of the battery.[21]

The success of commercial Li-ion rechargeable batteries was possible due to the correct selection of electrolyte materials that resulted in the formation of a stable anode-electrolyte interface,[22] known as the solid electrolyte interphase (SEI) as proposed by Peled.[23] This highlights how interfacial stability is crucial for battery development, becoming a bottleneck even when the ideal battery materials are chosen yet the battery interfaces prevent the optimum ionic or electronic transport, the correct adhesion among components, or the long term stability required for commercial battery operation.

The nature of the SEI has led to the use of different modeling approaches[24–30] and surface-specific experimental techniques for its characterization. Among the most widely used analytical techniques, ex situ[31] and in situ[32] Fourier transform infrared (FTIR) spectroscopy, Raman microscopy, and spectroscopy[33,34] along with refinements such as shell-isolated nanoparticles for enhanced Raman spectroscopy (SHINERS),[35] electrochemical quartz crystal microbalance (EQCM),[36] spectroscopic ellipsometry,[37] atomic force microscopy (AFM),[38] X-ray photoelectron spectroscopy (XPS)[39–41] including the use of the Auger parameter[42] or other charge correction methods[43] for peak assignment, nuclear magnetic resonance (NMR),[44] X-ray absorption spectroscopy (XAS),[45] soft X-ray absorption spectroscopy (sXAS),[46–48] and time-of-flight secondary ion mass spectrometry (ToF-SIMS)[41] have been utilized to investigate the properties and formation mechanisms of the SEI. The electrode-electrolyte interfaces for solid-state batteries have also been experimentally

M. Á. Muñoz-Márquez[+]
Centre for Cooperative Research on Alternative Energies (CIC energiGUNE)
Basque Research and Technology Alliance (BRTA)
Alava Technology Park, Albert Einstein 48, Vitoria-Gasteiz 01510, Spain
E-mail: miguel.munoz@unicam.it

M. Zarrabeitia, S. Passerini
Helmholtz Institute Ulm (HIU)
Helmholtzstrasse 11, 89081 Ulm, Germany
E-mail: stefano.passerini@kit.edu

M. Zarrabeitia, S. Passerini
Karlsruhe Institute of Technology (KIT)
P.O. Box 3640, 76021 Karlsruhe, Germany

T. Rojo
Departamento de Química Inorgánica
Universidad del País Vasco UPV/EHU
P.O. Box 664, Bilbao 48080, Spain
E-mail: teo.rojo@ehu.eus

The ORCID identification number(s) for the author(s) of this article can be found under https://doi.org/10.1002/admi.202101773.

[+]Present address: School of Science and Technology, Chemistry Division, University of Camerino, Via Madonna delle Carceri, 62032 Camerino, Italy

DOI: 10.1002/admi.202101773

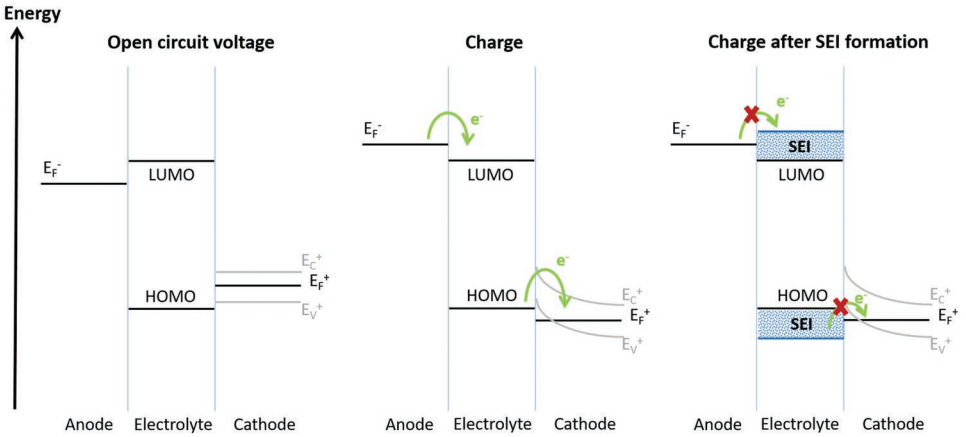

Figure 1. Energy diagrams of a rechargeable battery with metallic anode and semiconductor cathode. Both electrodes have a chemical potential that can be approximated to the Fermi energy of the anode (E_F^-) and the cathode (E_F^+). The latter having valence and conduction bands with energies E_V^+ and E_C^+, respectively. Left panel shows the energy levels of the system in thermodynamic equilibrium at open-circuit voltage. Central panel depicts the shifts of the Fermi energies upon charge. Right panel presents the final energy level rearrangement after the formation of the SEI.

characterized and studied computationally.[5] As a result, such studies of the SEI have improved the understanding of what governs the SEI formation, kinetics, and growth in Li-ion and Li-metal batteries. However, further studies are needed to identify a suitable SEI that does not grow over repeated cycling and does not dissolve at high temperatures.[21] The SEI of Na-ion batteries is of special interest because these batteries may complement Li-ion technology in the near future.[49,50]

2. The Solid Electrolyte Interphase

The formation of the SEI can be understood from the thermodynamical point of view by using energy band diagrams.[8,51] **Figure 1** depicts the SEI formation process starting from the open-circuit voltage state (left panel of Figure 1), in this case, and considering that the cell is under thermodynamical equilibrium, the chemical potential of the anode and the electrolyte lay within the electrochemical stability window of the electrolyte which, as first approximation, can be defined as the LUMO (lowest unoccupied molecular orbital) and HOMO (highest occupied molecular orbital) gap.[52] Therefore, no spontaneous reactions between electrode and electrolyte are expected. However, two important points have to be considered here: 1) the electrode chemical potential is equivalent to the Fermi energy at zero Kelvin, and it is often used to define the potential difference of an electrochemical cell, neglecting temperature and interfacial effects;[53] 2) the assumption of a system in thermodynamic equilibrium at open-circuit voltage is another approximation that neglects the spontaneous reactions of the electrode and the electrolyte as soon as the cells are assembled.[42] Upon charge (central panel of Figure 1), the electrons accumulate in the anode while they leave the cathode. Following this first-order approximation, results in an increase of the Fermi level of the anode (E_F^-) above the LUMO level of the electrolyte and in a decrease of the cathode Fermi level (E_F^+) below the HOMO level of the electrolyte. The new energy band distribution will lead to the spontaneous irreversible reduction of the electrolyte at the anode side and the irreversible oxidation of the electrolyte at the cathode side. The electrolyte decomposition can only be prevented by the formation of a suitable passivation layer (the SEI) in both electrodes that will block electron transfer after reordering the energy levels of the system (right panel of Figure 1).

It has to be noted that HOMO and LUMO are concepts defined within the electronic structure theory, that is, while investigating the electronic structure of isolated molecules not participating in redox reactions. On the other hand, redox potentials are directly linked to the Gibbs free energy difference of the chemical reactants and the resulting products in the redox process. For these reasons, the electrolyte stability should not be defined by the HOMO-LUMO gap, but by the potential of electrolyte reduction at negative potentials, and the potential of solvent oxidation at positive potentials (cf. **Figure 2**).[54]

The HOMO-LUMO gap has been shown in several cases to be a few eV broader than the electrolyte reduction-oxidation gap. Moreover, as described by Trasatti,[55] access to contact potential of the electrode–electrolyte interface and the electrode's work function is needed for the definition of the absolute electrode potential for both the anode and cathode. In

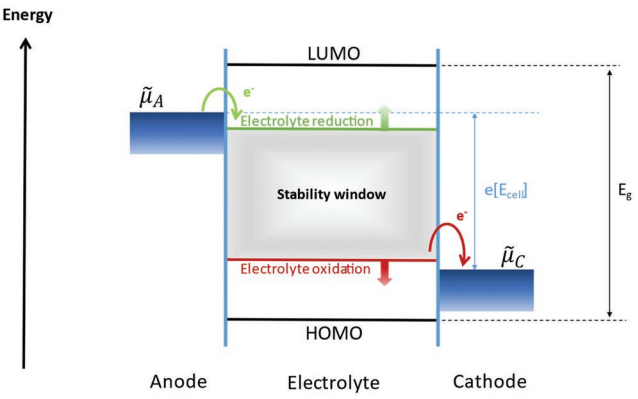

Figure 2. Electrolyte stability window defined in terms of potential of electrolyte reduction at negative potentials, and of the potential of solvent oxidation at positive potentials. Illustration is based on the information presented in ref. [54].

addition, these important parameters are necessary to understand the electronic properties and subsequent energy drive to electron transfer: a critical aspect of the electrolyte stability and for the functioning of electrochemical cells.[53]

From the practical point of view, the main drawback to achieve the ideal SEI is the difficulty to predict the reduction and oxidation reactions of the electrolyte occurring at the anode and cathode respectively. The other issue is the complexity to establish the structure-property relationships. In fact, the SEI remains one of the most poorly understood mechanisms in rechargeable Li-ion batteries due to the extreme complexity of the chemically and electrochemically driven reactions occurring to form the SEI and the lack of direct characterization of its physical properties.[8,56]

2.1. How to Name this Interphase?

In the literature, species formed in the contact region between electrode and electrolyte have been named differently. The first model and name was proposed by Peled in 1979[23] for non-aqueous battery systems of alkali and alkaline-earth metals that, as claimed by Peled, were always covered by a thin surface layer (15–25 Å thick) of insoluble products which was spontaneously formed upon contact of the metal with the electrolyte solution. This layer acts as an interphase between the metal and the electrolyte solution and has the properties of a solid electrolyte, that is, it is a good ionic conductor and a good electronic insulator. For this reason, the layer was called SEI.

After this, the studies of the SEI were mainly focused on the anodes for Li-ion batteries. This is because the low potential of anodes, such as metallic Li or graphite, operate below 1.0 V versus Li^+/Li which is outside the electrochemical stability window of most conventional non-aqueous electrolytes.[57] The operation below 1.0 V versus Li^+/Li results in the reduction of the electrolyte and subsequent formation of an overlayer in the anode surface that can either stabilize the cell operation after preventing further reactions of the electrolyte with the anode surface while increasing the cell impedance and decreasing its cycling efficiency,[58] or it forms a reversible interphase layer that negatively impacts the Coulombic efficiency and cycle life of the cell.

The stability of the electrolytes on the cathode side up to 4.5 V versus Li^+/Li was out of the range. However, the surface chemistry of oxide-based Li-ion cathodes was found to be more complex than expected triggering the decomposition/polymerization of carbonate ester-based electrolytes.[59,60] The study of the cathode surface chemistry and the application of the SEI model was further pursued by Edström and co-workers who introduced the concept of cathode-electrolyte interphase (CEI) in $LiMn_2O_4$ and $LiNi_{0.8}Co_{0.2}O_2$ cathodes for Li-ion batteries, that was also described by the same authors as a solid permeable interphase (SPI) layer:[61] where it is claimed that while the SEI in the anodes seems to degrade with slightly high temperatures and hence suffers from continuous reforming in the reduction cycles, the CEI thickness continuously increases with cycle number, storage time and, temperature losing its passivating ability. For this reason and considering the permeability of such cathode surface layer to electrolyte solvents and salts, the term SPI was chosen. Later, it was found that the $LiMn_2O_4$ surface modification, for instance through an Al_2O_3 coating, resulted in an improved electrochemical performance with a stable SPI that preserves the electroactive material dynamics.[62]

Later, Edström and co-workers, performed a comparative study of the electrode-electrolyte interphase composition in cathodes and anodes of a $LiFePO_4$/graphite Li-ion battery.[63] As shown in **Figure 3**, the inner parts of the anode SEI contain some species not observed in the thinner cathode SPI, particularly oxides and alkoxides. In contrast, the outermost anode SEI is somewhat similar to the cathode SPI, containing higher concentrations of C—H and C—O based compounds. Similar observations have been reported on the electrode-electrolyte interphases for $LiNi_{0.5}Mn_{1.5}O_4$ and graphite half-cells,[64] where the SEI is reported to be impermeable to the electrolyte solution in contrast with the SPI which is found to be permeable to electrolyte. The permeability of the SPI and easy accessibility of electrolyte molecules are one of the causes of the low Coulombic efficiency of $LiNi_{0.5}Mn_{1.5}O_4$.

Although different in compositional nature, the electrode-electrolyte interphases should have the same role in both anode and cathode: this is the blocking of electron transfer that triggers reduction or oxidation reactions while allowing ion mobility through the interphase layer. Therefore, this main role as solid electrolyte is one that should determine the name of the electrode-electrolyte interphase regardless of the solubility of the interphase components or the permeability of this interphase layer to electrolyte solvents and/or salts which, of course, are factors of crucial importance for battery performance. In other words, our proposal is to always use the term SEI when referring to the electrode-electrolyte interphase in the anode and CEI for the electrode-electrolyte interphase in the cathode. The interphase will have different compositional and physicochemical properties depending on the materials assembled in the cell; the permeability of the electrolyte is one of these properties that may or may not be present. However, recent experiments aimed at the direct determination of the CEI electronic character in Li-ion batteries have concluded that the electrode-electrolyte interface in the high voltage operating positive electrodes is an electronically conducting layer.[65] Therefore, the observed impedance increase on the positive electrode side should not be associated with the formation of an electronically insulating interphase, but it could be ascribed to an increment of the Li^+ diffusion resistance through the surface layer or with a degradation of the active material. Still, the role of the CEI is unclear and this will hinder the understanding of its physicochemical properties and subsequently, the selection of an appropriate name that defines the functionality of this layer.[51]

In the last years, the focus has been on the solubility of the SEI components upon cycling rather than on the permeability of the layers. This is evident for the SEI layers of Na-ion batteries which possess solubility problems.[66]

3. The SEI Models in Na-Ion Batteries

The SEI formation mechanisms remain a matter of debate with several formation models proposed through the years. The three most important SEI formation models are depicted with color in **Figure 4** (top panel): a) the Peled model which is the primary mechanism that defined the SEI formation as a result

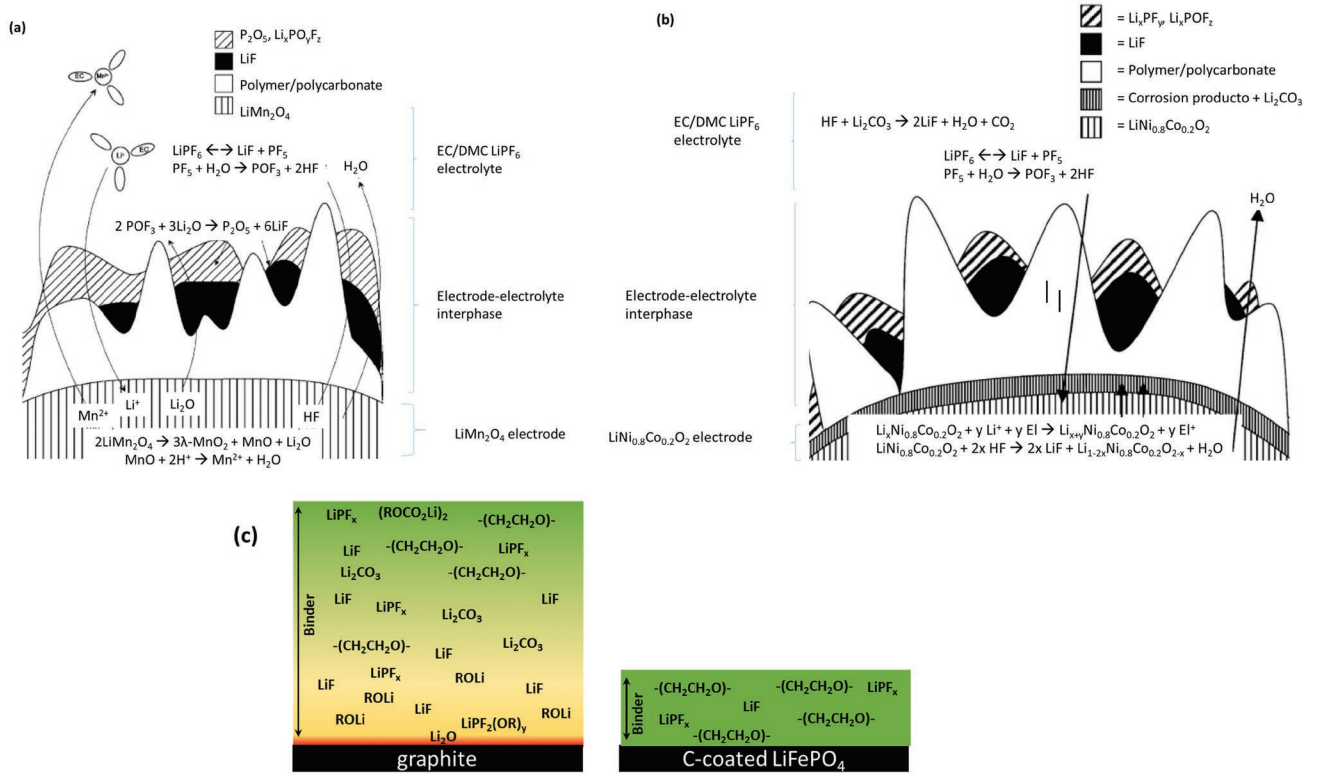

Figure 3. CEI composition of a) $LiMn_2O_4$ cathode, b) $LiNi_{0.8}Co_{0.2}O_2$ cathode, c) graphite anode and carbon-coated $LiFePO_4$ cathode as determined by photoemission electron spectroscopy. Reproduced with permission.[63] Copyright 2013, Elsevier.

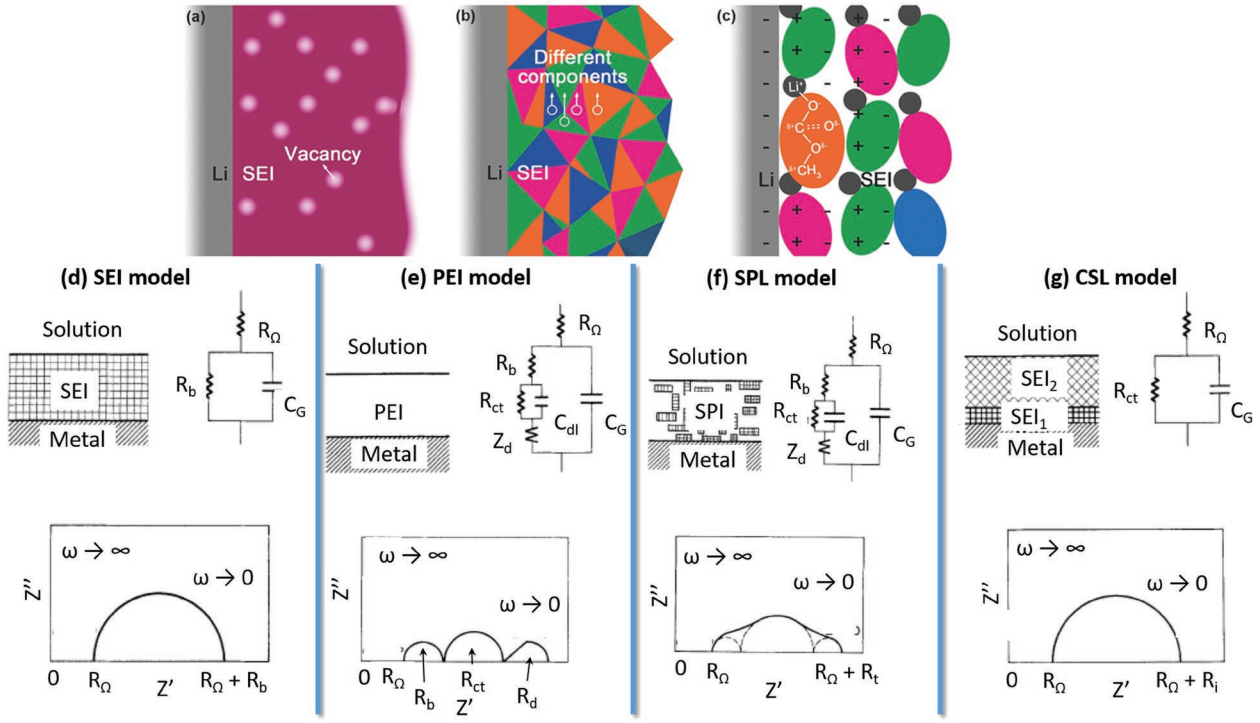

Figure 4. Schemes of the three mechanisms of SEI formation (top panel, color figures): a) the Peled model, b) mosaic model, c) Coulombic interaction mechanism. Schemes, impedance spectroscopy response, and equivalent circuit of the different structural SEI models (bottom panel): d) SEI model, e) PEI model, f) SPL model, and g) CSL model. a–c) Reproduced under the terms of the CC-BY 4.0 license.[209] Copyright 2015, The Authors, published by Wiley-VCH. d–g) Reproduced with permission.[210] Copyright 1987, The Electrochemical Society.

of a surface reaction of the electrode with the electrolyte, b) the mosaic model which is based on the Peled model and explains the SEI formation as a set of decomposition reactions that result in different insoluble components deposited on the electrode with a mosaic morphology that will allow the ions to move through the grain boundaries and, c) the Coulombic interaction mechanism model, where the SEI decomposition products are lined up forming a unique double layer that strengthens the components of the SEI resulting in the most stable SEI.

The SEI has been described using various models and equivalent circuits as shown in Figure 4 (bottom panel). Considering that the SEI is an electronic insulator and an ionic conductor, these are the different possibilities to represent this non-blocking system from the point of view of electrochemical impedance spectroscopy (EIS). The SEI model, Figure 4d, consists of a bulk resistance (R_b) and a geometric capacity (C_g) related to the layer conductivity. This simple model relates the thickness of the layer with the conductivity. The polymer electrolyte interphase (PEI) model is more complex, Figure 4e, and three different components are established: the conduction impedance defined by the R_b and the C_g, the charge-transfer impedance defined by the charge-transfer resistance (R_{ct}) and the double-layer capacitance (C_{dl}) and, the diffusion impedance (Z_d). The solid-polymer layer (SPL) model, Figure 4f, which assumes that the SEI consists of an intermix of solid compounds. In this case, the equivalent circuit can be the same used for the PEI model, however, different time constants of the conduction, charge-transfer, and diffusion processes will result in a different impedance spectrum that cannot be easily separated. Finally, the compact-stratified layer (CSL) model, Figure 4g, assumed an SEI made of two sublayers, where the first sublayer is a solid electrolyte on the electrode surface and the second one is a polymeric layer in contact with the electrolyte solution. Hence, the equivalent circuit would be the circuit of an SEI model in series with the circuit of another SEI or PEI model.

The knowledge obtained for the SEI of non-aqueous Li-ion batteries was subject to a revision when the first studies on the SEI of Na-ion batteries were performed by Komaba and coworkers on hard carbons[67] on the grounds of XPS in combination with ToF-SIMS experiments. This was also confirmed by Brandell and collaborators on organic electrodes by means of hard X-ray photoelectron spectroscopy (HAXPES),[68] where it was found that the Na-ion battery SEI is much thinner and richer in inorganic compounds than the Li-ion counterpart. Further synchrotron-based photoemission investigations by Edström's group reinforced the idea of an SEI divided into differentiated sublayers of organic- and inorganic-based nature.[69] Also, our research group determined that the SEI layer of Na-ion battery anodes such as $Na_2Ti_3O_7$, besides the reduced thickness of the interphase, was unstable upon electrochemical cycling.[42] This was attributed to the partial dissolution of the organic and semi-organic compounds. The differences in cell performance in terms of self-discharge and Columbic efficiency cannot fit into the 0.3 V difference in potential between Li and Na. It is has been suggested that the dissolution of the SEI components in Na-ion batteries is the main reason for the underperformance of this technology when compared with Li-ion batteries.[66] These results suggest that the Li-ion environment is less reactive and hence prone to form organic compounds. Moreover, this points towards the influence of the Na metal in the SEI formation and properties when performing half-cell experiments which were studied by our research group.[70]

For the study of the SEI properties in Na-ion batteries, a refinement of the models presented in Figure 4 was considered that had been successfully used in Li-ion battery electrodes (**Figure 5**).[71] The model is named the surface layer (SL) model, and was first proposed by Aurbach and was used to explain the Li^+ intercalation into graphite.[72] This model assumes an intercalation electrode with high electronic conductivity, as well as a compact enough electrode that ensures the contact between particles (solid-solid interface). After that, Barsoukov and coworkers, slightly modified the SL model, including R/C circuits in series to consider more realistic situations, such as non-uniform particle size, particle structure change, and new phase formation upon alkaline-ion insertion.[73]

The parameters that describe the alkaline-ion intercalation into porous electrode model including the SEI formation are R_{sol} which is the high-frequency intercept onto the real axis and corresponds to the Na^+ resistance across the electrolyte (solution); the high-frequency semicircle can be associated with a resistance and a capacitance of the SEI layer (R_{SEI} and C_{SEI}) in parallel which corresponds to the electric resistance of the Na^+ diffusion through the SEI layer and the double layer capacitance

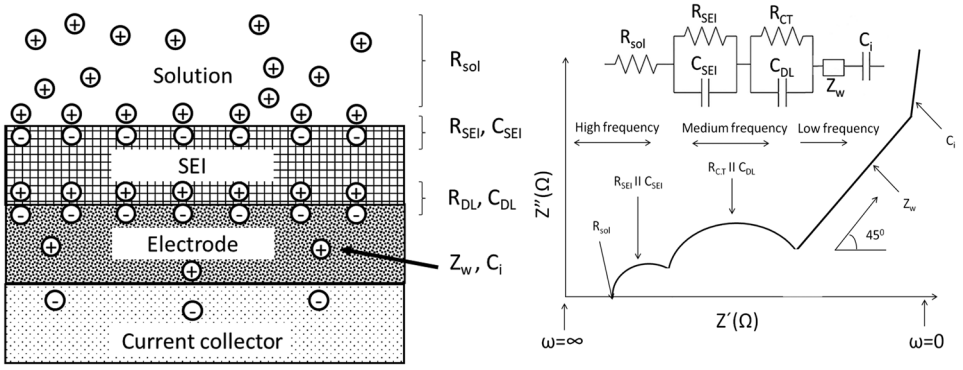

Figure 5. Scheme of the charge behavior in the electrode surroundings (left panel) and corresponding impedance spectroscopy equivalent circuit (right panel). The different contributions identified in the relevant interfaces of the left panel figure appear at different frequencies in the impedance spectroscopy experiments as noted in the right panel figure.

ascribed to the SEI-electrode interface; the medium-frequency semicircle is described by the R_{CT} and C_{DL} which correspond to the charge-transfer resistance of the Na^+ through the electrode surface and the double layer capacitance appearing in the electroactive material-electrolyte interface or in the electroactive material-SEI interface.[74] The sloping line in the lowest frequency region is the result of the solid-state diffusion of the Na^+ inside the electroactive material and can be considered as a Warburg diffusion element (Z_w)[75] in series with an intercalation capacity (C_i).[76] If the accumulation of charge at the electroactive material surface, or at intraparticle crystallite domains, is leading to a given capacitance (C_{elec}) along with an electronic resistance of the electroactive material (R_{elec}), an additional semicircle will appear in the low-frequency region overlapped with the solid-state diffusion features.[74] The aforementioned parameters, that is, R_{sol}, $R_{SEI}\|C_{SEI}$, $R_{CT}\|C_{DL}$, Z_w, and C_i are connected in series as indicated in the equivalent circuit in Figure- our model (right panel), due to the fact that the corresponding processes of each R/C circuits occur in series.

The SL model that describes the alkaline-ion intercalation through the SEI layer and the porous electrode can be compared and correlated with previously proposed models of the SEI layer (see Figure 4 – bottom). First, the SEI model assumes that the SEI is composed of inorganic compounds, but it has been experimentally proven that the SEI is composed of both inorganic and organic species. Nonetheless, the R_b and C_g proposed by the SL model might be equal to the R_{SEI} and C_{SEI}. However, the R_{SEI} and C_{SEI} also considered the electrode surface area (S), as well as the thickness (l), ionic conductivity/ resistivity ($\sigma = 1/p$) and permittivity (ε), see Equations (1) and (2).[77]

$$R_{SEI} = pl/S \tag{1}$$

$$C_{SEI} = \varepsilon S/l \tag{2}$$

Second, the PEI model assumes that the SEI is composed of polymeric and inorganic compounds, but the interphase has the polymer electrolyte properties. This is close to the assumption that the SEI behaves as a polymer electrolyte. However, the PEI model is not accurate since the alkaline ion resistance across the electrolyte and SEI occur in series, therefore the parameters of each process should appear in series and not in parallel. Third, the SPL model proposes a similar equivalent circuit as the PEI model, not considering that the process occurs in series. In addition, the assumption of SEI composition by SPL, that is, solid compound dispersed in a polymer electrolyte, is not experimentally observed. In fact, several studies report that the SEI is not homogeneously distributed, and it is composed of more than one layer, where each layer displays a different composition and properties. Finally, the CSL model approach of two sublayers, one solid close to the electrode and the other outermost composed by polymer compounds, is closer to the experimental observation, but the sublayer is not homogeneous and both types of species can be detected in the same sublayer. In this case, the equivalent circuit is the same as the one proposed by Aurbach and co-workers (SL model), since depending on the time constants of the processes, one or more R/C circuit/s in series will appear. In other words, when the time constant of the different processes occurs close (when frequency ratio (ω_1/ω_2) < 10) the Nyquist plot only exhibits one semicircle, which can include several processes and the equivalent circuit is composed of one R/C circuit, but when the time constant of the processes is different ($\omega_1/\omega_2 > 100$), each process exhibits one semicircle and the corresponding R/C circuit.

The impedance spectroscopy spectra can be fitted with Boukamp's Equivalent Circuit software,[78] ZView,[79] etc. so for each EIS spectrum a set of R_{sol}, R_{SEI}, C_{SEI}, R_{CT}, C_{DL}, Z_w, C_i, R_{elec}, and C_{elec} will be obtained. In the fitting procedure, the Z_w and C elements can be replaced with constant phase elements (CPE) that will account for deviations from the ideal interfacial behavior such as inhomogeneities and roughness.[75] If a series of EIS measurements are carried out at many different states of charge during charge and discharge, each one of the obtained EIS spectra can be individually fitted using, for example, the Boukamp's software. Hence obtaining the different resistance and capacity values during cycling,[74,80] which will provide a dynamic picture of the electrochemical behavior and in particular of the SEI evolution.

4. The SEI/CEI in Na-Ion Battery Electrodes

The family of electrode materials that have been developed in the last decades for Na-ion batteries is rather broad, including transition metal layered oxides ($Na_xTM_yO_2$, TM = one or more metal/s),[81–83] polyanionic compounds,[84,85] Prussian blue analogs (PBAs)[86] and organic compounds[87,88] as cathodes and hard carbons,[89–91] soft carbons,[92] sodium titanates,[93,94] alloys,[95] and also PBAs[96] as anodes. However, very few of them have reached the prototype/demonstrator level. In 2013, Sumitomo Chemical Co. Ltd. developed a pouch cell prototype of Na-ion battery using hard carbon as anode and O3-type $NaNi_{0.3}Fe_{0.4}Mn_{0.3}O_2$ as cathode, delivering 650 mAh.[97] In 2015 several Na-ion cell prototypes were released worldwide using hard carbon as anode: Sharp Laboratories of America, Inc. reported a Na-ion cell prototype in combination with a Prussian White cathode,[98] Faradion Ltd. developed a 126 Wh kg^{-1} cell using Ni-based layered oxide,[99] that culminated with the deployment of a 400 Wh Na-ion battery pack used to power an e-bike.[100] Also in 2015, the French electrochemical energy storage network (réseau sur le stockage électrochimique de l'énergie, RS2E) announced the first 18 650 cell prototype of a Na-ion battery delivering 90 Wh kg^{-1} over 2000 cycles that was acquired by Tiamat company.[101,102] In 2017, Sharp Laboratories of America, Inc. filed a patent of a hard carbon anode,[103] the same year, Sharp Laboratories of Europe published the results of a 4.2 Ah cell with an energy density of 252 Wh l^{-1} that consisted of a hard carbon anode and a $NaNi_{1/3}Fe_{1/6}Mn_{1/3}Mg_{1/12}Sn_{1/12}O_2$ cathode.[104] All the investigations carried out at Sharp Laboratories of America and some of their researchers started the spin-off Novasis Energies Inc. that developed Na-ion battery prototypes based on PBAs as cathode and hard carbon as anode, reaching energy density values in the range of 100–130 Wh kg^{-1} or 150–210 Wh l^{-1}.[100] In 2018, HiNa Battery technology Co. in China released a low-speed car powered by a Na-ion battery.[105,106] After this, in 2019, HiNa Battery installed a 30 kW/100 kWh large-scale energy storage system

based on O3-type $Na_{0.9}[Cu_{0.22}Fe_{0.30}Mn_{0.48}]O_2$ cathode and hard carbon anode chemistry.[107] Recently, Contemporary Amperex Technology Co Ltd (CATL) successfully integrated Na-ion cells and Li-ion cells into one pack, based on Prussian White as cathode and hard carbon as anode, with the advantages of high energy density (Na-ion battery cell up to 160 Wh kg^{-1} – 2nd generation up to 200 Wh kg^{-1}), fast-charging capability (80% in 15 min at room temperature), excellent thermal stability, great low temperature (limit at –20°C) and high integration efficiency (>80%). In parallel, CATL has started the industrial deployment of Na-ion batteries, and plans to form a basic industrial chain by 2023.[108] However, despite all the efforts on the development of a suitable Na-ion battery prototype, issues such as the SEI formation were overlooked. This is a very important factor that has a significant impact on the battery in terms of electrochemical performance and cost.[109]

The surface specificity of XPS has made this technique one of the better suited and most widely used to study the SEI and CEI components and chemical species as well as its stability. XPS consists of an incident X-ray beam that illuminates the material under study down to a depth in the µm range. The incident photons will induce the emission of photoelectrons from the core levels of the atoms present in the material. Due to their short inelastic mean free path, only the photoelectrons emitted from the outermost surface atoms (few nanometers depth) will be able to leave the material under study and travel to the photoelectron detector. The kinetic energy of the detected photoelectrons can be correlated with the binding energy of the electron energy level in the atom. Since the binding energy is a unique feature of each element, the analysis of the photoelectron spectra will allow the identification of the elemental composition of the material surface. Slight energy shifts of the binding energy can be used to evaluate the chemical environment of the elements. Of course, this technique has its own limitations: 1) the analysis has to be carried out under ultrahigh vacuum conditions, unless the system is based on a solid electrolyte or a liquid electrolyte with very low vapor pressure and with a particular architecture/thickness that allows photoelectrons from the SEI to travel through the electrolyte. All XPS analysis will have to be carried out ex situ, which involves careful sample handling to avoid surface reaction with air; 2) the use of X-ray photons that are in the 1 to 3 keV energy range for laboratory-based XPS and can go up to 12 keV in synchrotron-based XPS may lead to photon-induced reactions of the material under study and subsequent modification of the surface composition; 3) the removal of electrons from the material under study might lead to surface charging effects that are translated into artificial shifts of the binding energy, hence rendering extremely difficult the XPS peak interpretation. Regarding this last point, the consistent use of references is very important for the correct interpretation of the XPS data. In **Figure 6** the most relevant SEI compounds in Na-ion batteries are shown in terms of the binding energies of the C 1s, O 1s, F 1s, and Na 1s photoelectron lines. In the figure, there is not a unique binding energy value for every single component and there is a slight tolerance in the values that depends on several factors such as electronic conductivity of the species and the existence of non-stoichiometric phases. For this reason, the compounds presented in Figure 6 are assigned to a range of binding energies instead of having a single binding energy value.

4.1. SEI/CEI Formation with Carbonate Ester-based Electrolytes

The carbonate ester-based electrolytes have been the model electrolytes in Li-ion battery technology. They possess excellent ionic conductivity values and are the electrolyte of choice in commercial Li-ion batteries. Due to their success, versatility, and ease of use, these electrolytes have also been adopted in Na-ion batteries.

The carbonate esters solvents can be classified into cyclic and linear: propylene carbonate (PC) and ethylene carbonate (EC) are cyclic carbonate esters with dielectric constants in the ≈65 to ≈90 range, viscosities at room temperature above 2.5 cP and close to 2cP, HOMO levels around –0.25 eV and LUMO levels close to –0.015 eV; dimethyl carbonate (DMC), ethyl methyl carbonate (EMC), and diethyl carbonate (DEC) are linear carbonate esters with dielectric constants around 3, viscosities at room temperature in the 0.59 to 0.75 cP range, HOMO level around –0.25 eV and LUMO levels in the –0.009 to –0.003 eV.[128] Typically, cyclic and linear carbonate ester-based solvents are mixed so as to tune the viscosity while improving ionic conductivity and electrochemical stability.

In this context, the most common salts for carbonate ester-based electrolytes are $NaClO_4$, $NaPF_6$, NaTFSI, NaFSI, and NaFTFSI. Among them, $NaClO_4$ and $NaPF_6$ are widely employed in research despite the risk of explosion of the former and the water sensitivity that leads to HF formation of the latter salt. For example, NaTFSI and NaFSI are more thermally stable but they are highly corrosive and tend to damage the Al current collectors used in Na-ion batteries.[129]

In terms of additives to ameliorate the interphase, only fluoroethylene carbonate (FEC) has been effective in enhancing the cycling performance.[130] Other additives used in Li-ion batteries with good results such as ethylene sulfite (ES), vinylene carbonate (VC), and difluoroethylene carbonate (DFEC) have not worked in Na-ion batteries.[130–133] The most relevant results regarding SEI/CEI characterization are presented below and summarized in Table S1, Supporting Information.

4.1.1. Negative Electrodes

Hard Carbons: The electrochemical response of carbon against Na was reported in 1993 by Doeff and co-workers,[134] in 2000, Stevens and Dahn reported the Na^+ insertion in hard carbons[135] which was resumed by Komaba et al. 10 years ago.[67] Hard carbon is one of the negative electrodes for Na-ion batteries that has reached prototype level, however, its application in battery production at the industrial level has been negatively affected by its high initial irreversibility, poor rate performance, and long-term cycling degradation typically ascribed to the continuous consumption of electrolyte and SEI growth.[110,111] The role of the SEI in hard carbons has been studied for more than a decade. During this time, the common belief is that the hard carbon capacity fade is due to the continuous SEI formation,

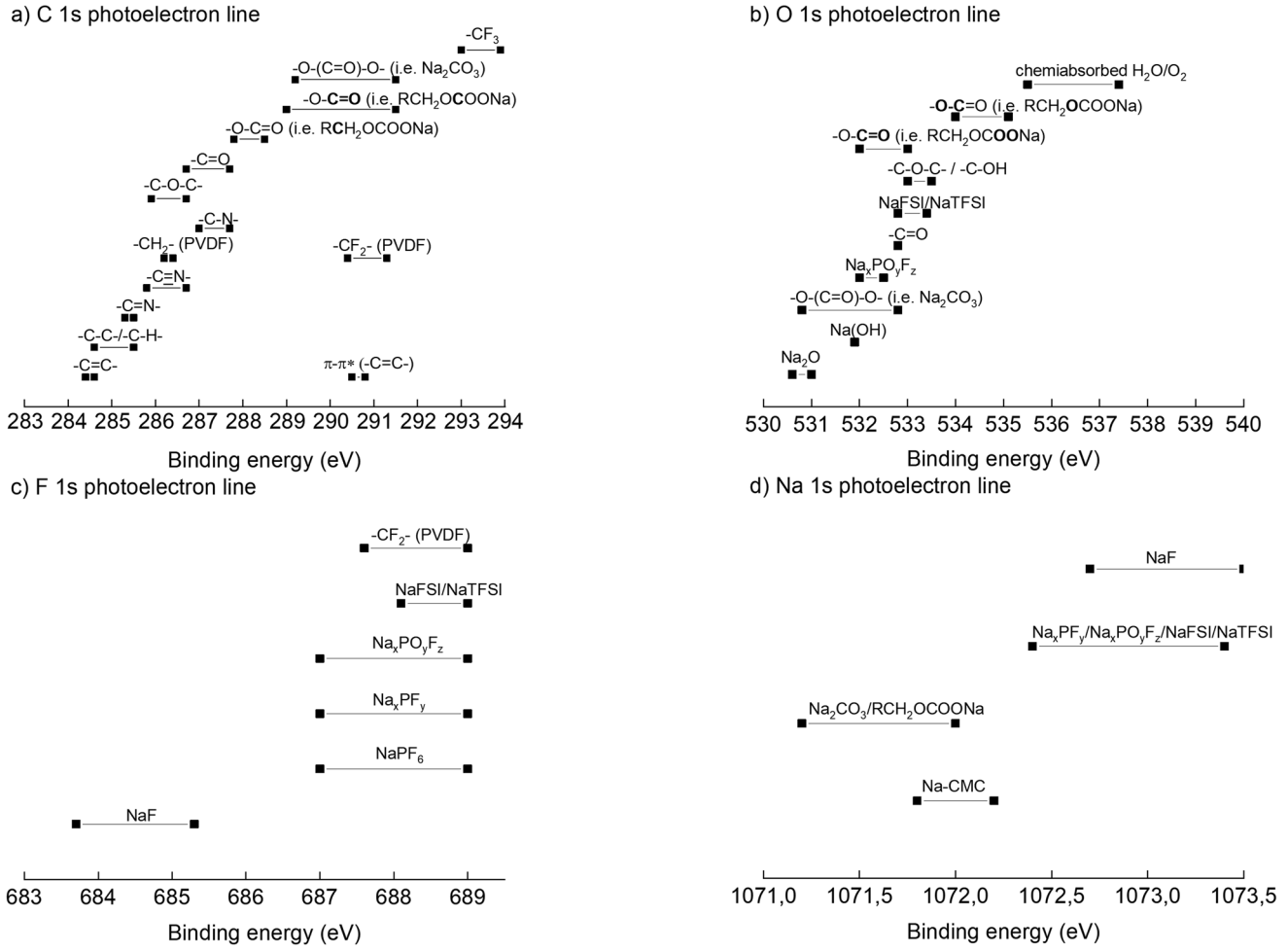

Figure 6. Experimental photoelectron binding energy references used to assign the XPS peaks to the different compounds. The most common SEI compounds for Na-ion batteries are included in four different photoelectron lines: a) C 1s, b) O 1s, c) F 1s, and d) Na 1s. The binding energy values have been obtained from refs. [42,67,70,110–127].

however, there are other experiments that point to a particular inward SEI progression towards the anode instead of the conventional outward growth. This SEI growth effect on the hard carbon capacity fade is presented along with the influence of metallic Na as counter electrode.[136] On the other hand, the influence of the hard carbon precursors in the SEI composition has been recently studied on three hard carbons synthesized from three different precursors namely, phenolic resin, polyethylene fibers, and lignin-rich biomass.[137] The tests in Li- and Na-half-cells have concluded that, other than the hard carbon precursors, the SEI chemical composition is influenced by the solubility of the SEI species. The SEI in Li-ion cells was composed of organic and inorganic species, where the concentration of the inorganic species increases in the SEI subsurface, close to the electrode, while the SEI layer in Na-ion cells was mainly formed by carbon/oxygen-containing species. The sodium electrolyte salts were marginally found in the SEI sublayer, due to their high solubility in the electrolyte upon electrochemical cycling and washing procedure. These results suggest that the sample preparation of the cycled electrodes for the ex situ characterization experiments in Na-ion systems is significant, more so than for Li-ion systems. In 2016 a thorough XPS study concluded that the passivation films formed upon contribution from FEC electrolyte additive can lead to an improvement of the capacity retention resulting in a better passivation of the SEI. The use of $NaPF_6$ salt in combination with FEC in PC-based electrolyte results in the optimum passivation of the hard carbon electrode with polyvinylidene difluoride (PVdF) binder that ultimately leads to the enhancement of the cycling performance.[112] Nonetheless, it has been observed that hard carbon electrodes with carboxymethyl cellulose (CMC) binder do not need FEC additive to deliver high reversibility and cycling stability, as well as a good passivation SEI.[118] The electrode and electrolyte formulation and their combination are essential to define the electrochemical and SEI properties of the system. Recent studies of the SEI were performed on hard carbon electrodes in Na half-cells with two different salts ($NaPF_6$, NaTFSI) and two different electrolyte additives FEC and fluorinated dimethylcarbonate (DMCF) in a mixture of EC and DMC solvents. The best electrochemical performance was delivered by the $NaPF_6$ salt together with 3% FEC. The DMCF additive was found to have a detrimental

effect in all combinations. As determined by XPS, the SEI composition based on sodium ethylene dicarbonate and NaF was ascribed to the best electrochemical behavior, while the worst electrochemical performances were associated with low NaF or high Na_2CO_3 containing SEIs.[111] In stark contrast with the positive effect of FEC, previous studies have reported the detrimental effect of FEC additive in terms of specific capacity and Coulombic efficiency.[138] In parallel, it has been found by other authors[139] that the combination of NaTFSI salt with 3% FEC in PC electrolyte for hard carbon half-cells delivers electrochemical performance comparable to the best combination, namely $NaPF_6$ with 3% FEC in a mixture of EC:DMC. Moreover, the SEI in the NaTFSI-based electrolyte stabilizes its physicochemical features after 10 cycles when the NaF and Na_2CO_3 concentration increases in the organic-inorganic hybrid SEI.[139]

Alloys: Alloy compounds have been considered as alternative negative electrodes for Na-ion batteries, as high storage capacity and low voltage operating materials. Among the various semimetals candidates from group 14 (Si, Ge, Sn, and Pb) that will form NaX- and $Na_{15}X_4$-type compounds, Sn has been postulated as the most promising due to its theoretical capacity of approximately 847 mAh g^{-1} (assuming the full conversion into $Na_{15}Sn_4$).[125] Meanwhile, group 15 elements (P, As, Sb, and Bi) will form Na_3X-type compounds, with phosphorous being the element delivering alloying reactions with the highest specific capacity (2596 mAh g^{-1}). However, the main disadvantage of alloy compounds is their poor cycling stability due to the continuous volume changes upon (de)sodiation hindering the formation of a stable SEI.[140] In this context, the SEI chemical composition and properties have been examined by several groups on various Sn- and Sb-based alloys, such as Sb, Cu_2Sb, and SbSn.[124,126,127] The reported works highlight that the electrode and electrolyte formulation as well as their combination govern the formation of a stable SEI. Bodenes and co-workers compared the SEI chemical composition and stability on Sb electrodes cast with two different binders, namely PVdF and CMC, in Na- and Li-ion systems, highlighting that the SEI thickness is related to the binder nature, while the chemical composition depends on the chemistry, that is, Li- or Na-ion.[126] As it has been shown for hard carbons, the Na/CMC formulation was better suited than Na/PVdF.

Intermetallic Sb_x—M_y alloys have been developed as a strategy to mitigate the volume changes of alloy-based electrodes. For instance, SnSb alloys have been reported as feasible anodes for Na-ion batteries,[141] although the SEI formation was only inferred from the profile of the charge/discharge galvanometry. Instead, the SEI of SnSb nanoparticles, which were encapsulated in porous carbon nanofibers, has been investigated using FEC electrolyte additive.[127] It has been observed that the presence of FEC prevents the electrolyte decomposition and leads to the formation of a thin and uniform SEI; once in half-cell configuration the FEC positive effect was confirmed. The beneficial effect of FEC additive on the SEI stability has also been confirmed for Sn electrodes where the additive enables the extended cycling of Sn-polyacrylate electrodes.[142] Commercial intermetallic InSb alloys have demonstrated good electrochemical performance as anodes for Li-ion batteries,[143] in terms of structural stability and electrochemical reversibility. The InSb alloy has also been tested in Na-ion batteries with 1M $NaClO_4$ in EC:DMC (1:1) and 5% FEC as electrolyte,[144] while delivering 450 mAh g^{-1} after 50 cycles at C/5 and 310 mAh g^{-1} at 5C. The SEI on the InSb electrode was studied by means of XPS that revealed that the SEI is based on FEC and salt degradation products such as NaF and $NaClO_3$. Some organic species deriving from carbonate degradation were also evidenced, yet they partially dissolve on charge.

The theoretical capacity of red phosphorous (P) has always been considered as one of the most viable anodes for Na-ion batteries. However, sodium storage in red P anodes is limited by significant technical challenges such as poor conductivity, large volume swelling, and unstable SEI therefore they have yet to be implemented in batteries.

Regarding the SEI on red P anodes, it tends to crack upon Na cycling resulting in freshly exposed electrode surface, hence promoting the continuous growth of the SEI layer and leading to low Coulombic efficiency and large electrode resistance.[145] However, the use of FEC additive on 1M $NaClO_4$ in PC can improve the SEI structural stability.[146] The effects of using or not using the FEC additive on the composition of the formed SEI in each case were studied by means of hard- and soft-X-ray photoemission spectroscopy.[145] This study demonstrated, for the FEC-containing electrolyte, the formation of $(PO_4)^{3-}$, P^0, Na_xP, and NaH_2PO_2 species in the subsurface SEI while $(PO_4)^{3-}$ and NaH_2PO_2 are the only species observed in the outermost SEI, which suggests that Na_3P reacts with the SEI and the electrolyte to form the P^+-based species. Of course, NaF and Na_xP-F_yO_z species resulting from the fluorinated additive are also formed. Meanwhile, the FEC-free electrolyte led to the formation of an SEI completely free of P^0 and Na_xP species, instead, alkyl carbonate ($ROCO_2Na$) ester-based species appear.

Sodium Titanates: In the family of sodium titanates, $Na_2Ti_3O_7$ is considered the most promising negative electrode, due to its low voltage redox reaction (0.3 V vs Na/Na^+) and its composition based on Earth-abundant elements.[147] However, it suffers from poor capacity retention,[148] which is tied to the inadequate combination of electroactive material, electrolyte, and binder which does not result in a stable SEI that suffers from $ROCO_2Na$ dissolution as determined by XPS and Na-Auger parameters.[42] In the same study, it was concluded that the ≈5 nm thick SEI has a bilayer structure with an inner layer of inorganic compounds such as Na_2CO_3, NaF, and NaCl, covered by a semi-organic overlayer of polyethylene oxide (PEO) and $ROCO_2Na$. The inorganic components, namely, NaCl and NaF are formed after spontaneous decomposition of the electrolyte salt in contact with Na metal and by the PVdF dehydrofluorination, respectively: confirming the higher reactivity of Na if compared with Li. These results largely expanded the ex situ high-resolution TEM (HRTEM) investigation carried out by Pan et al. that revealed the instability of the 2–5 nm thick SEI and the negative influence of the fluorinated binder on the electrode cyclability.[149] This work also reported based on ab initio calculations, the insulator to electronic conductor transition of the $Na_2Ti_3O_7$ upon electrochemical cycling. Later, the SEI instability and the electroactive material conductivity changes were directly determined by means of EIS measurements,[74] where the electroactive material resistance and the oscillations of the SEI layer resistance with the state of charge were identified and the latter associated with the $ROCO_2Na$ dissolution and the breaking of the layer itself.

The impact of Na metal on the electrochemical performance and SEI formation was evaluated by comparing the $Na_2Ti_3O_7$ electrode in half-cells with Na metal and full-cells using $NaFePO_4$ as the cathode.[70] It was concluded that, although the SEI composition was similar in both cases, the full-cell SEI was slightly thinner, the spontaneous reactions observed in half-cells were almost negligible in the full-cell configuration. This highlights the importance of full-cell studies to understand the SEI formation behavior, without neglecting the half-cell studies that are always a good starting point. The $ROCO_2Na$ dissolution observed in half-cells was also detected in full-cells, thus indicating that the metallic Na is not responsible for the $ROCO_2Na$ behavior.

On the other hand, the CEI formed on the $NaFePO_4$ positive electrode, in terms of composition is similar to the SEI formed on the $Na_2Ti_3O_7$ negative electrode; but with lower thickness, around 2.5 nm, as determined from the graphitic component intensity change in the C 1s XPS data and considering the Tanuma´s equation for photoelectron inelastic mean free paths.[150]

4.1.2. Positive Electrodes

The non-aqueous liquid electrolytes generally used in Li-ion technology are oxidized at operating voltages >4.5 V versus Li^+/Li.[151] Considering that the equilibrium potential of Na^+/Na is 0.3 V above that of Li^+/Li, it is reasonable to deduce that the carbonate ester-based electrolytes will be thermodynamically unstable above ≈4.2 V versus Na^+/Na in Na-ion batteries.[152] Given that many of the cathode materials used in Na-ion batteries have their redox activity totally or partially above this oxidation limit; progress is needed for the design of new electrolytes that can withstand the required (higher) voltages.

Prussian Blue Analogs: Prussian blue with general formula $Na_xTM[Fe(CN)_6]_y \cdot \gamma_{1-y} \cdot nH_2O$ (TM = transition metal and γ = $Fe(CN)_6$ vacancy), are interesting cathode materials for Na-ion batteries due to their high theoretical capacity and low-cost. However, the high number of $Fe(CN)_6$ vacancies and crystal water generated by current synthesis routes lead to limited cyclability.[153,154] In contrast, very recent investigations on Prussian blue with a considerable number of $Fe(CN)_6$ vacancies and crystal H_2O point towards a low cyclability due to the CEI instability. In fact, the addition of cresyl diphenyl phosphate (CDP) to the 1M $NaClO_4$ dissolved in EC/DEC (1:1 volume ratio) with 8% FEC can effectively suppress the interface side reactions between the Prussian blue and the electrolyte and extend the cycle lifetime with a capacity retention of 83.1% after 700 cycles at 1C.[155] This enhanced interface stability is ascribed to the formed overlayer which is composed of some phosphates that originated from partial CDP decomposition on the Prussian blue surface during cycling. The formed phosphates, specifically $FePO_4$, activate the low-spin Fe ions during cycling, which is also beneficial for the extended cycle life of Prussian blue in Na-ion batteries. In general, the kinetics of Na-ion batteries are known to struggle owing to the solid-state diffusion of Na^+ in the intercalation host. This problem also appears in PBA-based electrodes, however, this bulk-related drawback can be tackled by a surface modification approach such as the controlled etching of the Prussian blue surface that results in the activation of new Na storage sites and the stabilization of the CEI while improving the Na^+ diffusion dynamics.[156] Other authors have reported the importance of having significant concentrations of Na_2CO_3 in the Prussian blue CEI.[157] In this work, they compared the electrochemical performance of two Prussian blue cathodes synthesized using the same route but with different water content. This water reacts with the $ROCO_2Na$ present in the CEI leading to the formation of Na_2CO_3. The CEI with a higher concentration of Na_2CO_3 helps to enhance the cycling stability and rate performance by providing the electrodes with better protection and facilitating the charge-transfer process as determined by FTIR and EIS. Again, this result contradicts the argument that crystal water hinders the cyclability of Prussian blue cathodes. Moreover, the presence of Na_2CO_3 in the CEI of aqueous Na-ion batteries was reported to be beneficial,[158] whereas in non-aqueous systems the presence of Na_2CO_3 in the CEI is detrimental for electrochemical performance. Besides the higher solubility of Na-ion CEI components with respect to Li-ion CEI, in particular, the solubility of Na_2CO_3 in organic solvents is much higher than the one of Li_2CO_3: 6.603 mg L^{-1} in PC and 3.648 mg L^{-1} in EC:DEC for Na_2CO_3, 0.160 mg L^{-1} in PC and 0.135 mg L^{-1} in EC:DEC for Li_2CO_3.[159]

Polyanions: Among the polyanionic materials, the $Na_4CO_3(PO_4)_2P_2O_7$ positive electrode exhibits multi redox couples at high voltage, between 4.1 and 4.7 V, and a specific capacity of 95 mAh g^{-1} at 0.2C in the 3.0–4.7 V versus Na^+/Na voltage window with a capacity retention above 95% over 100 cycles, as reported by Toyota Battery Research division in 2013.[160] The chemical composition and stability of the formed CEI are of extreme importance considering that the high operating voltage of this electrode material is around the stability limit of most conventional carbonate ester-based electrolytes. Recent investigations on the grounds of EIS and XPS reveal the formation of a bilayer CEI after full desodiation (4.7 V vs Na^+/Na),[80] with semi-organic-rich compounds in the inner CEI region (close to the electrode surface) while the organic compounds are mostly accumulated in the outer CEI region facing the electrolyte. Meanwhile, after full sodiation (3.0 V vs Na^+/Na), an additional outermost inorganic overlayer, ≈10 nm thick, is formed on the CEI. This inorganic overlayer is mainly composed of Na_2CO_3 and Na_xPF_x and it dissolves upon oxidation/desodiation while during reduction/sodiation it is reformed. In the meantime, the other CEI sublayers remain stable.

Among the NASICON ($Na_3M_2(XO_4)_3$); X = Si^{4+}, P^{5+}, S^{6+}, Mo^{6+}, As^{5+}) framework materials, which are well known for their facile Na^+ conductivity. $Na_3V_2(PO_4)_3$ has an impressive theoretical energy density of 400 Wh kg^{-1} with good thermal stability in the charged state,[161,162] that has been shown to report excellent cycling stability, rate capability, and Coulombic efficiency.[163] The modification of the material morphology has resulted in a CEI with reduced impedance, as determined by EIS, that, despite not having details on its composition and distribution, has certainly contributed to the observed improvement of the electrochemical performance.[164] At the same time, the N-doping of the carbon matrix introduced with $Na_3V_2(PO_4)_3$ decreases electroactive material polarization by facilitating the charge-transfer at the electrode-electrolyte interphase.[165]

Besides the investigations performed on surface modifications or doping of the $Na_3V_2(PO_4)_3$ electrodes, a thorough study of the CEI in half- and full-cells is still required.

$Na_3V_2(PO_4)_2F_3$ is considered by part of the scientific community as the exemplary material for the cathode of commercial Na-ion batteries.[166] This polyanionic compound has outperformed some P2- and O3-type layered oxides in full-cells assembled with hard carbon anodes, with the layered oxides falling behind the polyanion due to their intrinsic phase transformations and volume changes. However, not all layered oxides were considered in this study, for instance, P2-type layered oxides doped with Ti with general formula P2–$Na_{2/3}Mn_{0.8}Fe_{0.2-x}Ti_xO_2$ deliver outstanding electrochemical performance with Ti buffering structural distortions.[167] Nonetheless, $Na_3V_2(PO_4)_2F_3$ still suffers from limited Coulombic efficiency and cyclability. The use of conventional liquid electrolytes in $Na_3V_2(PO_4)_2F_3$ half-cells has resulted in the formation of an unstable and extended CEI that hinders the electrochemical performance and could only be partially improved by the use of FEC or VC additives,[168] still delivering low capacity retention: ≈44% at 25 °C and ≈34% at 60 °C after 500 cycles. In full-cells with hard carbon, it has been shown that the soluble species formed in the SEI from the presence of linear ester carbonates in the electrolyte can shuttle to the cathode affecting the long-term cyclability.[169] This result would suggest limiting the use of linear carbonates like DMC, DEC, etc. in favor of the cyclic ones such as PC, EC, etc., in stark contrast with the latest studies that report the best electrochemical response of $Na_3V_2(PO_4)_2F_3$ half- and full-cells with hard carbon in the 0 to 50 °C range for the electrolyte with the highest linear carbonate content: 1M $NaClO_4$ in 1:1 PC:DMC with 5% FEC additive.[170]

Layered Oxides: The layered oxides with general formula $NaTMO_2$ (TM = Ti, V, Cr, Mn, Fe, Co, Ni, and a mixture of 2 or 3 elements) offer many advantages due to their simple structure, high capacities, and relatively easy synthesis.[81,171] According to the classification by Delmas, these layered oxides are typically found in trigonal prismatic (P) or octahedral (O) coordination for the Na and with a different number of unique interlayers surrounded by different oxide layers, in other words, typically 2 or 3 transition-metal layers in a single cell unit.[172] The most common arrangements are P2-, O3- and P3-type phases. In this context, single TM layered oxide systems such as Na_xTiO_2, Na_xCrO_2, Na_xMnO_2, Na_xFeO_2, Na_xCoO_2, etc. were developed in the early 1980's and although in some cases exhibit excellent cyclability in an acceptable voltage range, these systems have been used as the basis for more complex compounds. Exploring in detail the single and binary TM systems would be beyond the scope of this review, for this reason we will focus on the more recent ternary systems. In particular, Mn-based materials meet the requirements for low-cost stationary batteries without sacrificing energy density or safety. Therefore, herein we will focus on Mn-based materials.

O3-type phases are preferred because of the high Na content that would permit the use of a Na-free negative electrode and also exhibits an improved 1st charge capacity. However, after the 2nd cycle, the P2-type phases show better electrochemistry because of the low diffusion barrier and high ionic conductivity.

O3-type $NaNi_{0.6}Co_{0.05}Mn_{0.35}O_2$ has demonstrated ≈157 mAh g^{-1} specific capacity at 15 mA g^{-1} in half-cells and 125 mAh g^{-1} with 80% retention over 300 cycles in full-cells.[173] The cycling of this cathode in hard carbon full-cells with 1M $NaPF_6$ in EC:DMC (30:70) with 2% FEC in the 2 to 4.2 V range results in the formation of a mixed O3-P3 phase that takes place in the 4.0 to 4.2 V range after 50 cycles.[174] TEM investigations have concluded that this phase transformation only occurs in the outermost ≈20 nm of the electroactive material surface and it also affects the chemical composition, particularly Na deficiency, Mn dissolution, and TM reduction. This change in the surface composition will drive the formation and evolution of the CEI which has been found to be rather inhomogeneous and composed of fluorinated species, $ROCO_2Na$, and Na_2CO_3 as determined by XPS.

The combination of Ni, Mn, and Co has also displayed interesting cycling stability and specific capacity in P2-type layered oxides. P2-type $Na_xCo_{2/3}Mn_{2/9}Ni_{1/9}O_2$ when cycled in half-cell with 0.5M solution of $NaPF_6$ in PC with 5% FEC additive in the 2.0–4.2 V range can reach 89% capacity retention after 90 cycles with a Coulombic efficiency >99.4%. Nevertheless, despite displaying a high specific capacity of 140 mAh g^{-1}, the electrochemical performance of this material drops when charged to 4.5 V versus Na^+/Na. Therefore, a key point to study will be the chemical reactions at the electrode-electrolyte interface which will partly depend on the electrolyte stability at high voltages and the electronic structure of the cathode material. The transition metal oxidation state in the electroactive material surface and the CEI evolution of this system have been studied by means of HAXPES and XPS, respectively.[121] The HAXPES experiments have determined that whilst the transition metals in the pristine electrode surface are in the Mn^{4+}, Ni^{3+}, and Co^{3+} state with traces of Co^{4+}, in the first charge to 4.5 V, only Ni and Co are active and oxidize to Ni^{4+} and Co^{4+}. During discharge at 3.5 V, these two cations were initially reduced to Ni^{3+} and Co^{3+} while a further voltage decrease to 2 V resulted in activation of Mn being reduced to Mn^{3+} together with the partial reduction of Ni and Co to Ni^{3+} and Co^{3+}. After the 2nd charging cycling, all cations were oxidized to 4+ state. This analysis confirms that the plateaus observed in the electrochemical charge/discharge profile do not necessarily correspond to a given redox couple. As for the CEI composition, NaF, Na_2CO_3, and traces of oxygenated and carbonaceous species are present in the pristine electrode, prior to any contact with the electrolyte. Once the cell is assembled and the electrolyte introduced, the electrode overlayer remained intact. It was during charge that NaF and Na_2CO_3 were slowly disappearing and reappearing during discharge. Meanwhile, the oxygenated and carbonaceous species were not affected during cycling. $NaPF_6$ and other degradation products are part of the CEI, the detailed analysis of the outermost surface region confirmed that phosphates were the main degradation product at low potential while fluorophosphates were the dominant degradation product at high voltages.

Of course, if the focus application of Na-ion batteries is for large-scale energy storage, suppressing the use of Co is of paramount importance.

One of the Co-free layered oxides is the distorted O3-type $NaMnO_2$ which, as with all Mn-containing layered oxides can suffer from water and/or CO_2 adsorption when exposed to air and Mn^{3+} disproportionation. Both of these effects being dramatic for the material degradation and capacity fade. The Ti enrichment-induced surface reconstruction in distorted

O3-type $NaMnTi_{0.1}Ni_{0.1}O_2$, can lead to many benefits.[175] The all-titanium surface layer effectively prevents the contact between the Mn species and environmental conditions and suppresses the disproportionation reaction of manganese: $2Mn^{3+} \rightarrow Mn^{4+} + Mn^{2+}$. This Ti^{3+}-rich overlayer with spinel-like structure and atomic-scale thickness boosts the electron and ion conductivity while significantly increasing the chemical/electrochemical/thermal stability with impressive specific capacity of (186 mAh g^{-1}), rate capability (118 mAh g^{-1}, 1000 mA g^{-1}, 5C rate), and cycling stability.

P2-type $Na_{2/3}Mn_{0.8}Fe_{0.1}Ti_{0.1}O_2$ layered oxide with a voltage cut-off of 4.0 V versus Na^+/Na is a promising Co-free cathode material made of Earth-abundant transition metals that delivers 156 mAh g^{-1} with 90% capacity retention after 100 cycles. When cycling in half-cells using 1M $NaPF_6$ in EC:PC with 2 wt.% of FEC additive as electrolyte, the CEI consists of fluorinated species ($NaPF_xO_y$ and NaF), mainly observed at reduced state, while at the discharged (oxidized) state the fluorinated layer is covered by carbonaceous species such as PEO, Na_2CO_3, and $ROCO_2Na$. The latter species being highly soluble in the electrolyte, thus dissolving during desodiation, and providing an unstable CEI.[176]

Recently, the sodium deficiency of P2-type $Na_{2/3}Mn_{0.8}Fe_{0.1}Ti_{0.1}O_2$ layered oxide and its intrinsic 1st cycle irreversible capacity loss has been addressed using $Na_2C_3O_5$ as sacrificial salt to compensate for the lack of Na.[177] This results in the formation of a thin CEI with the same composition as the CEI formed in cells without sacrificial salt. The CEI thickness could be a consequence of the salt decomposition, during which CO_2 gas is released while "breaking" and/or creating cracks along the interphase formation. In addition, the alkoxides formed on the negative electrode diffuse through the electrolyte to react with the CO_2 formed at the positive electrode while filling the cracks in the interphase, thus resulting in a more stable CEI.

4.2. SEI/CEI Formation with Advanced Electrolytes

Considering the limited success of carbonate ester-based electrolytes in Na-ion batteries, the scientific community strongly focused on the development of advanced electrolytes; the ether-based and the ionic liquids are amongst the most explored.[128,178] Other solid or quasi-solid electrolytes are also hot topics of Na-ion battery research such as gel polymer, solid polymer, and inorganic solid electrolytes,[179–181] as well as, organic ionic plastic crystals (OIPCs) which are the solid counterpart of ionic liquids.[182] However, in terms of interface characterization, the solid or quasi-solid electrolytes still remain a challenge for the state of the art surface characterization techniques. Therefore, we will only review the SEI studies performed with advanced liquid electrolytes, namely ether-based and ionic liquids.

In Li-ion batteries, ether-based electrolytes have never been regarded as a viable candidate.[183] In contrast, they have offered interesting properties in terms of SEI formation for Na-ion batteries.[184,185] Ether-based electrolytes, also known as glymes, have been studied for use in Na-ion batteries since 2010. Ether-based electrolytes (1M NaOTf in diglyme) allow the Na^+ co-intercalation into graphite, enabling the possible use of graphite anode for Na-ion batteries.[186]

Ionic liquids were first synthesized in 1914 by Walden,[187] and if small molecular ionic liquids are considered, they generally have large-size low-symmetric organic cations and small-sized inorganic anions. The representative anions are TFSI–, FSI–, BF_4–, PF_6–, SbF_6–, AsF_6–, $C_4F_9SO_3$–, CF_3SO_3–, $(CF_3SO_2)_2N$–, CF_3COO–, C_3F_7COO–, $(C_2F_5SO_2)_3C$–, $(C_2F_5SO_2)_2N$–, FSA, etc. The cations usually are [PYrr], [PYri], [RRIm], $[NR_xH_{4-x}]$, or $[PR_xH_{4-x}]$ types. All ionic liquids are characterized by low vapor pressure, non-volatility, the adjustability of polarity, wide liquid phase range, high inherent conductivity, wide electrochemical window, as well as dual solvent and catalyst functions.[178] Ionic liquids were first tested in Li-ion batteries, and now new ionic liquid electrolytes are being developed for Na-ion batteries to enhance the electrochemical performance of the different electrodes such as alloys, polyanionic compounds, layered oxides, etc.[188–193] The most relevant results regarding SEI/CEI characterization on advanced electrolyte systems are presented below and summarized in Table S1, Supporting Information.

4.2.1. Negative Electrodes

Hard Carbon: As mentioned in section 4.1.1, hard carbon is the most studied anode material for Na-ion batteries. Therefore, it is also the electrode in which the most advanced liquid electrolytes have been tested. Carbonate ester-based electrolytes formed a thick SEI that could be further stabilized by using FEC additive. Meanwhile, the SEI formed on hard carbon anodes cycled with 1M $NaCF_3SO_3$ (NaOTf) in diethylene glycol dimethyl ether (DEGDME) resulted in the formation of a thin SEI that improved the initial Coulombic efficiency and cycling stability if compared with the same system cycled in 1M $NaClO_4$ in EC/DEC.[194] The diglyme electrolyte performed much better than the carbonate esters for the first charge/discharge cycle: 320 mAh g^{-1} at 0.1C with 63% initial Coulombic efficiency for the diglyme and 280 mAh g^{-1} with 41% initial Coulombic efficiency for the carbonate ester-based. The superior performance of the diglyme was even more significant at high C rates: 217 mAh g^{-1} at 3C for the diglyme which is almost 3.5 times higher than the 61 mAh g^{-1} delivered by the carbonate ester-based cell at the same rate. The ether-based SEI is compact but dense enough to prevent further decomposition of electrolytes when in contact with the electrode. At the same time, the reduced thickness of this SEI facilitates fast Na^+ diffusion which results, as described above, in very good response at high C rates. With extended cycling, that is, 2000 cycles and beyond, the capacity of the diglyme system dropped substantially to ≈70 mAh g^{-1}. The extraordinary efficiency of the diglyme-based system was later combined with the stability of the carbonate ester-based SEI. In other words, the thick SEI for the hard carbon was formed using a carbonate ester-based electrolyte. Once the SEI was formed, the cell was disassembled and reassembled using diglyme-based electrolyte so as to take advantage of the efficiency of the ether-based electrolyte while operating with unprecedented reversibility.[195] The ester-based SEI is thicker and will therefore result in lower Coulombic efficiency in the first cycle and higher resistance to Na^+-transport, leading to

slow kinetics. However, the mechanical properties of the ester-based SEI are much better than for diglyme-based SEI. The Young's modulus of the SEI as determined by AFM nanoindentation is one order of magnitude lower for the ester-based SEI, in the range of polymeric materials, which involves an improved mechanical compliance to allow for volume changes in the long cycling. The XPS observations conclude that the diglyme-based SEI is thinner and with an elevated concentration of inorganic species which would agree with the higher Young's modulus measured.

The ionic liquids, such as sodium bis(fluorosulfonyl)amide (Na[FSA]) dissolved in N-methyl-N-propylpyrrolidinium-FSA ([C_3C_1pyrrr][FSA]) have stable operation in a wide temperature range and deliver superior electrochemical performance. Na[FSA]-[C_3C_1pyrrr][FSA] was found to be suitable for use on hard carbon electrodes exhibiting a reversible capacity of 260 mAh g^{-1} at 90 °C.[196] The irreversible capacity observed in the first cycle is attributed to the formation of the SEI. The EIS measurements at mid-frequency are consistent with a charge-transfer process at the electrode-electrolyte interphase. Since the charge-transfer resistance is much larger than the electric resistance, the cell resistance can be approximated with the R_{CT} which, after increasing with decreasing temperature, would indicate a significant sensitivity to the temperature of the SEI.

On hard carbons, more in depth studies of the SEI have been performed with other ionic liquids such as sodium bis(trifluoromethylsulfonyl)imide (Na[FSI]) dissolved in 1-butyl-1-methylpyrrolidinium-FSI ([Pyr_{14}][FSI]) electrolyte has been analyzed and compared to the behavior observed with carbonate ester-based electrolytes (cf. **Figure 7**). XPS experiments determined the SEI thickness in this system to be thin (<7 nm), well below the thickness reached with carbonate ester-based electrolytes. Moreover, in the ionic liquid-based SEI few inorganic-based compounds are present, with NaF the main inorganic species, with high concentrations of hydrocarbons and C—N-based species, the latter from $[Pyr_{14}]^+$ decomposition reactions.[197] The $[Pyr_{14}]^+$ contribution found in the subsurface region suggests that the SEI is porous. The SEI composition in the ionic liquid-based system is prone to be insoluble therefore the SEI is more stable.

Alloys: The suitability of InSb alloy as anode for Na-ion batteries was first demonstrated using ionic liquid-based electrolytes Na[FSA] dissolved in N-methyl-N-propylpyrrolidinium bis-(fluorosulfonyl)amide ([Pyr_{13}][FSA]),[198] before carbonate ester-based electrolytes were utilized. This cell with Na[FSA]-[Pyr_{13}][FSA] was more stable than the one with carbonate ester-based electrolyte, delivering capacities of over 400 mAh g^{-1} for 250 cycles. However, the SEI in this system requires further study to ascertain the difference in cycling performance.

Dahbi and co-workers tested the red P electrodes with ionic-liquid electrolyte, NaFSI in N-methyl-N-propylpyridinium-bis-fluorosulfonylamide ([MPP][FSA]), and compared their electrochemical performance against cells assembled with carbonate ester-based electrolytes, namely 1M $NaPF_6$ in EC:PC:DEC, EC:DEC, and PC electrolyte solvents.[122] Just as hard carbon electrodes in ionic liquid-based electrolytes, the capacity retention of red P improves with respect to the carbonate ester-based ones. This capacity retention increase was attributed to the different chemical compositions of the formed SEI. HAXPS and ToF-SIMS experiments revealed that the SEI layer formed with ionic liquid electrolyte onto P mainly consists of inorganic species, originating from the decomposition of MPP^+ cations and FSI^- anions which form a homogenous and stable surface layer during the first cycle that effectively passivated the P electrode. Meanwhile in carbonate ester-based electrolytes the continuous growth of the SEI up to the 20th cycle was observed, leading to poor electrochemical performance.

Sodium Titanates: $Na_2Ti_3O_7$ is the most promising material within titanates due to their low Na voltage insertion. For this reason, its performance has been also tested using NaFSI in [C_3C_1pyrr][FSI] ionic liquid in a 2:8 molar ratio at 90 °C in half-cell configuration.[199] The $Na_2Ti_3O_7$ delivers 215 mAh g^{-1} as the first charge capacity, which is above its theoretical capacity (178 mAh g^{-1}),[147] with an initial Coulombic efficiency of 51%. The large irreversibility on the first cycle was attributed to the formation of the SEI, as occurs when this electrode is tested in carbonate ester-based electrolytes. Despite the higher initial charge capacity for ionic liquid-based cells than in carbonate ester-based electrolytes (≈150–200 mAh g^{-1}), the $Na_2Ti_3O_7$ still suffers from poor long-term stability, displaying a poorer capacity retention for ionic liquid-based cells. The EIS, XRD, and SEM experiments indicate that the poor long-term stability of $Na_2Ti_3O_7$ is due to the insulator nature of the material, suffering from sluggish Na^+ insertion/extraction kinetics. The SEI formed with ionic liquid electrolytes is stable upon electrochemical cycling, as suggested by the unchanged high-frequency semicircle in the EIS measurements. Therefore, it can be concluded that, for the $Na_2Ti_3O_7$, the capacity retention is not enhanced by developing an optimum electrode-electrolyte configuration but by modifying the material itself.

4.2.2. Positive Electrodes

Prussian Blue Analogs: The interfacial side reactions and Na dendrite growth typically observed in PBA-based Na-ion batteries that rely on conventional carbonate liquid electrolytes can be suppressed by a polymerized FEC that results in a semi-solid state Na-ion battery with a reinforced PBA-electrolyte interface, which achieves an ultra-long lifetime of 3000 and 4000 cycles at 1 and 2C, and high-rate capacity of 121 mAh g^{-1} at 1 C and 88 mAh g^{-1} at 10C.[113] Besides, the use of ionic liquids with PBAs for Na-ion batteries has yet to be explored. However, there are some studies on Ca-ion[200] and Zn-ion batteries[201] where the use of PBAs along with ionic liquid-based electrolytes is exploited. Considering the interesting behavior of PBAs as electrodes for Na-ion batteries, the role of ionic liquids in these systems requires additional exploration.

Polyanions: The $Na_3V_2(PO_4)_2F_3$ and $Na_3V_2(PO_4)_3$ polyanions have been tested using 1M $NaPF_6$ in diglyme using Na metal, hard carbon, or $Na_3V_2(PO_4)_3$ as anode (counter) electrode.[202] In contrast with the observations gathered from the same electrochemical couples in carbonate ester-based liquid electrolytes, the diglyme electrolyte permits the use of Na metal as counter/reference electrode, due to the fact that the diglyme is reductively stable against Na metal. The diglyme reduction stability was further studied by considering the possible gas evolution

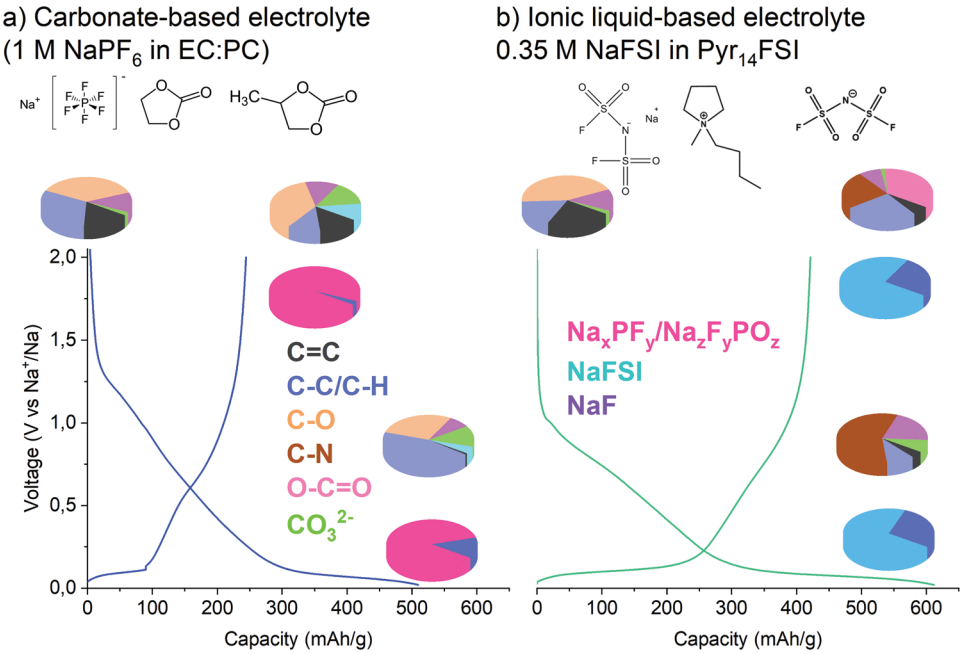

Figure 7. Voltage profile of the 1st cycle and the concentration of the SEI species obtained by fitting C 1s and F 1s photoelectron lines of hard carbon negative electrode tested in a) carbonate ester-based (1M $NaPF_6$ in EC:PC) and b) ionic-liquid (0.35M Na[FSI] in $[Pyr_{14}][FSI]$) electrolyte.

upon time, where no gas evolution was observed in contrast with the gas formation detected for 1M $NaPF_6$ in ED:DMC (1:1). Westman and co-workers suggested that the absence of gassing may be linked to the CEI stability. The $Na_3V_2(PO_4)_2F_3$|Na half- and $Na_3V_2(PO_4)_2F_3$|hard carbon full-cells exhibit a Coulombic efficiency of ca. 99.5% and 99%, respectively. The lower Coulombic efficiency in the full-cell is limited by the hard carbon desodiation irreversibility, which was further confirmed by the excellent Coulombic efficiency achieved by the $Na_3V_2(PO_4)_2F_3$|$Na_3V_2(PO_4)_3$ full-cell.

The mechanism of CEI formation (**Figure 8**) has been studied on $Na_3V_2(PO_4)_3$ using $NaPF_6$ salt dissolved in imidazole-based ionic liquid 1-butyl-3-methylimidazolium bis (trifluoromethanesulfonyl) imide ([BMI][TFSI]).[203] In general, it has been demonstrated that this electrolyte with high thermal stability (>350 °C) reduces the flammability of the cell, hence increasing the safety. The existence of free $TFSI^-$ and $[Na(TFSI)_2]^-$ in the electrolyte was predicted by DFT simulations and confirmed by Raman spectroscopy. Meanwhile, the oxidative decomposition of the free $TFSI^-$ resulted in the compounds later forming the CEI, namely Na_2SO_4, $Na_2S_2O_7$, and NaF as detected by means of EDS, XPS, and FTIR. The CEI layer was evident after one cycle, becoming more homogeneous and stable after 20 cycles. The hydrolysis of Na^+ in the electrolyte generates NaOH which is also detected in the CEI.

$Na_3V_2(PO_4)_2F_3$ cells cycled with Na[FSA]-$[C_3C_1pyrr][FSA]$ have demonstrated excellent cyclability as well as an enhanced rate capability at high temperatures: 105.6% capacity retention after 500 cycles with an average Coulombic efficiency of 99.8% at 25 °C and 90.5% capacity retention with an average Coulombic efficiency of 99.2% at 60 °C. This excellent electrochemical performance is the result of the thin and robust CEI formed after the oxidation of FSA^- in the ionic liquid electrolyte at different temperatures, as suggested by XPS and EDX measurements.[168]

The influence of highly concentrated $[FSA]^-$-based ionic liquid electrolytes such as Na[FSA]–$[C_2C_1im][FSA]$ and Na[FSA]–$[C_3C_1pyrr][FSA]$ on the rate capability and cycle life of $Na_2FeP_2O_7$ positive electrodes has been studied up to mid-temperature. At around 90 °C, the electrode retained 93% of its initial capacity while cycling at 1 A g^{-1}, almost full discharge capacity is obtained at 4 A g^{-1}, and 79% of the capacity is retained at 20 A g^{-1}. In the 25 to 90 °C temperature range, a very high Coulombic efficiency above 99.5% is found at 100 mA g^{-1} for more than 300 cycles.[204] The increase of the temperature or the Na salt fraction promotes the formation of lower coordination environments for Na^+, for instance $[Na[FSA]_2]^-$ which will influence the reactivity of the electrolyte with the electrode surface. Raman spectroscopy investigations have demonstrated that the interfacial chemistry on the electrode surface can be altered by changing the Na^+ local coordination. Considering that the desolvation energetics drive the ion transfer behavior at the electrode-electrolyte interface,[205] the weak interaction between Na^+ and FSA^- is supposed to facilitate the Na^+ insertion reaction thus improving the resulting battery performance. As demonstrated by EIS experiments, the Na[FSA]–$[C_2C_1im][FSA]$ results in charge-transfer resistance values two times lower than those observed in the Na[FSA]–$[C_3C_1pyrr][FSA]$-based system. Therefore, it can be concluded that the Na^+ diffusion in the electrolyte and the electron transfer at the electrode-electrolyte interface is superior for the Na[FSA]–$[C_2C_1im][FSA]$-based system, leading to enhanced electrode kinetics. Nevertheless, the structural changes and the interface also impact the Na^+ diffusion.

The former phosphate ($Na_2V_2(PO_4)_3$) and the pyrophosphate ($Na_2FeP_2O_7$) have been tested with phosphonium cation OIPCs

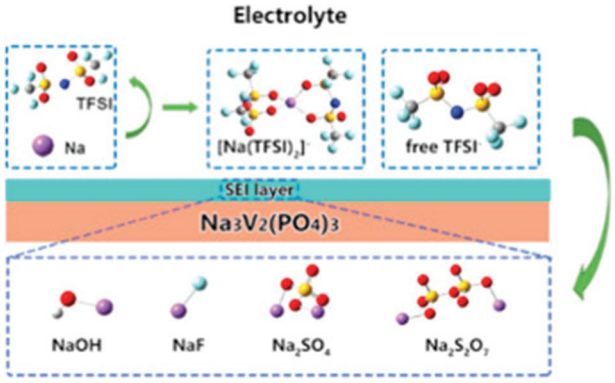

Figure 8. The reaction steps of the electrolyte $NaPF_6$-[BMI][TFSI] with the $Na_3V_2(PO_4)_3$ electrode that led to the formation of the CEI. Reproduced with permission.[203] Copyright 2018, Elsevier.

based on FSI^- and $TFSI^-$ mixed with Na salts, which are the solid counterpart of ionic liquids with all their advantages complemented with high ionic conductivities.[206] These advanced electrolytes allow the operation of the cell at high temperature with better performance in terms of current density, polarization, capacity, and rate capability than at room temperature. This is due to the higher ionic conductivity of the bulk electrolyte and a higher level of electron transfer occurring at the electrode surface at high temperature, as confirmed by the evolution of the charge-transfer resistance at the electrode-electrolyte interface during EIS experiments.

Layered Oxides: Several layered oxides have been studied in ether-based electrolytes in half- and full-cell configuration, in all cases they displayed a satisfactory electrochemical performance. For example, the P2-type $Na_{0.7}CoO_2$|$NaClO_4$ in TEGDME|Graphite full-cell delivers high Coulombic efficiency, long cycle life -80% capacity retention at 10C over 1200 cycles- and outstanding high power density (45% of the maximum capacity is obtained discharging in 6 min) with an average voltage of 2.2 V.[207] However, few works have been carried out on the CEI study of layered oxides with this type of electrolyte. Among them, the O3-type $NaNi_{0.6}Co_{0.05}Mn_{0.35}O_2$ layered oxide cycled in hard carbon full-cells with high-concentration ether-based electrolyte: 1.2M NaFSI in dimethoxyethane (DME) with (bis(2,2,2-trifluoroethyl) ether (BTFE) outperforms the carbonate ester-based electrolyte system discussed in Section 4.1.2. In the 2–4.2 V range, this cathode delivers good cycling stability with ≈83% capacity after 100 cycles in the advanced electrolyte, contrasting to the 72% after 50 cycles in the conventional electrolyte.[174] With this advanced electrolyte, the O3-P3 surface phase transition is one order of magnitude thinner than the observed carbonate ester-based electrolyte. Also the CEI is slightly thinner, 3 nm for the advanced electrolyte and 4 nm for the conventional one, and with a different composition absent of carbonates and alkyl carbonates and with a marked increase of NaF.

The CEI formation using ionic liquid electrolytes has also been investigated in the layered oxides. Gomes Chagas and co-workers compared the electrochemical performance of P2-type $Na_{0.45}Ni_{0.22}Co_{0.11}Mn_{0.66}O_2$ half-cells in 0.5M $NaPF_6$ in PC and 0.45M NaTFSI in $Pyr_{14}FSI$ at room temperature.[208] The main difference between both systems is the cycling stability and specific capacity, showing higher values in ionic liquid- than in carbonate ester-based electrolytes. The P2-type $Na_{0.45}Ni_{0.22}Co_{0.11}Mn_{0.66}O_2$ in PC solvent delivers 90 mAh g^{-1} with a Coulombic efficiency of 97.8% after 100 cycles and a capacity retention of 40%. Meanwhile, when using ionic liquid electrolytes 177 mAh g^{-1} are delivered with a Coulombic efficiency of 98.7% and 80% capacity retention. The higher Coulombic efficiencies and cycling stability with ionic liquid electrolytes have been attributed to the absence of Mn dissolution in the electrolyte and on the other hand, the formation of a thin but uniform CEI that covers the active material and carbon conductive additive, as indicated by post-mortem SEM images. In contrast, the cycled electrode in PC shows agglomeration of particles, a non-uniform layer with a rough surface and high porosity, indicating a continuous formation and potentially a partial dissolution of the CEI.

Another in-depth study of the CEI formation and composition has been carried out with similar ionic liquids, that is, 0.45M [NaFSI]-[Pyr_{14}][FSI], using the P2-type $Na_{0.67}Mn_{0.8}Fe_{0.1}Ti_{0.1}O_2$ layered oxide as cathode. The formed CEI has been investigated by means of XPS and compared to that formed in carbonate ester-based electrolyte (**Figure 9**).[176] The CEI in this P2-type cathode using ionic liquids has some similarities to the SEI observed in hard carbons when using the same ionic liquid electrolyte. The CEI thickness is found to be lower than in carbonate ester-based electrolytes. While the CEI chemical composition mainly consists of organic species as observed in hard carbon—such as hydrocarbons and C—N-based species. Meanwhile, less inorganic compounds are observed, such as SO_x and NaF. The NaF formation in the cathode side is even less pronounced than in the anode side, suggesting that the NaFSI might be stable in this configuration. Finally, the CEI in the ionic liquid-based system is more stable upon electrochemical cycling, which may be due to the formation of decomposition products that are less soluble.

The practical applications of ionic liquid using layered oxides as cathode and hard carbon as anode has been also investigated by Wang and co-workers, as well as the formation of the CEI/SEI in both electrodes and compared with the one formed in carbonate ester-based electrolyte.[190] The $Na_{0.44}MnO_2$|1M NaFSI in N-propyl-N-methylpyrrolidinium (PMP)–FSI |hard carbon full-cell overcomes the electrochemical performance obtained by carbonate ester-based electrolyte, delivering 117 mAh g^{-1} at 0.1C with a Coulombic efficiency of 99% and a capacity decay of 3% after 100 cycles at 25 °C. The superior electrochemical performance using ionic liquid electrolyte has been investigated by post-mortem SEM images, illustrating that the SEI formed on the hard carbon electrode is dense while CEI is negligible on the $Na_{0.44}MnO_2$ cathode side. However, in the carbonate ester-based system the electrode-electrolyte interphase is more pronounced on both sides, showing a high concentration of decomposed products also in the cathode. In addition, XPS experiments were performed for the P2-type $Na_{0.45}Ni_{0.22}Co_{0.11}Mn_{0.66}O_2$ cathode with the CEI determined to be composed of hydrocarbons in ionic liquid media. Meanwhile the CEI formed on carbonate-based electrolyte is full of O—C=O and Na_2CO_3 species, suggesting that the formation of $ROCO_2Na/Na_2CO_3$ is detrimental for the stabilization of the CEI and for optimal electrochemical performance.

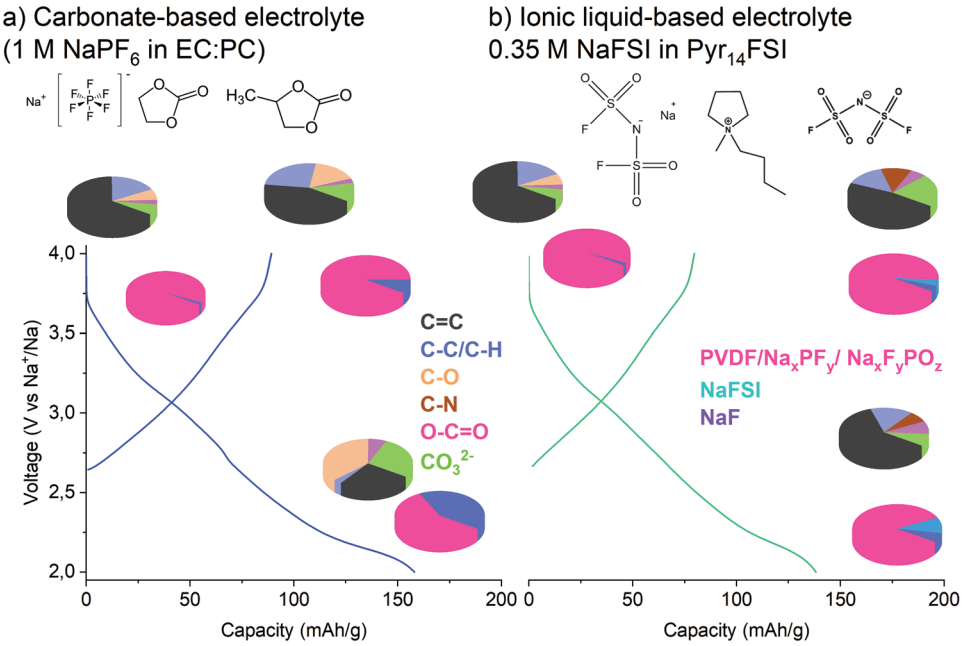

Figure 9. Voltage profile of the 1st cycle and the concentration of the CEI species obtained by fitting C 1s and F 1s photoelectron line of P2-type $Na_{2/3}Mn_{0.8}Fe_{0.1}Ti_{0.1}O_2$ positive electrode tested in a) carbonate ester-based (1 M $NaPF_6$ in EC:PC) and b) ionic-liquid (0.35 M NaFSI in $[Pyr_{14}][FSI]$) electrolyte.

5. Conclusions

Tailored electrode and electrolyte materials may lead to the development of advanced Na-ion batteries that meet the requirements for electric vehicles and renewable energy storage. However, in general, the combination of such components, namely electrode and electrolyte, and the subsequent formation of a stable interface between them is essential for the superior electrochemical performance of the battery. This electrochemical investigation must be performed with a consideration of the physicochemical properties driving the surface and interface chemistry in an electrochemical cell. Particular attention must be paid to revising critical concepts such as the absolute electrode potential, the modeling of the charge-transfer phenomena, and the ultrafast ion and electron dynamics at the electrode surface. This will only be possible using model systems that are similar to those used commercially and if the experimental characterizations of the surfaces and interfaces can provide information of the system under real operating conditions.

From the studies performed on the SEI/CEI of Na-ion batteries, one can conclude that Na-ion technology could be competitive with Li-ion technologies if a suitable composition of binders, carbonate-based electrolyte, additives, and electroactive materials is realized, along with a feasible cell design. However, the quest for a suitable electrolyte is required to bring the Na-ion technology to the market. The available knowledge from the Li-ion technology can be of help to design the electrolytes for Na-ion batteries, but the direct and full transfer of knowledge is not granted. For instance, ether-based electrolytes are rarely used in Li-ion batteries due to their stability problems in the cathode surface above 4.0 V versus Li^+/Li or their low passivation ability on the anode side. In stark contrast, ester- and ether-based organic electrolytes are the most promising for Na-ion batteries, due to their advantages such as high ionic conductivity, great wettability towards electrode and separator and, low cost. Indeed, ether-based organic electrolytes in Na-ion batteries have shown to be more resistant against reduction on the anode side while leading to a thinner SEI offering higher Coulombic efficiency, which is well beyond that obtained with ester-based electrolytes. Both types of organic electrolytes, namely ester- and ether-based, still display significantly high fire hazards, which is the main drawback for battery applications. In the long term, the commercial feasibility of ionic liquids will have to be assessed. Currently, the ionic liquid-based electrolytes are sometimes considered as a high-cost solution that delivers back safety, environmental friendliness, and electrochemical efficiency. There are no obvious reasons to think that, with the adequate upscaling plan, ionic liquid electrolytes cannot be cost-competitive, thus becoming electrolytes of choice for future Na-ion batteries.

Supporting Information

Supporting Information is available from the Wiley Online Library or from the author.

Acknowledgements

This work was supported by the Ministerio de Ciencia, Innovación y Universidades [PID2019- 107468RB-C21]; and the Gobierno Vasco/Eusko Jaurlaritza [IT1226-19]. M.Z. and S.P. also thank the Helmholtz Association for the financial support. Hyein Moon is acknowledged for sharing hard carbon XPS data in carbonate ester-based electrolyte.

Conflict of Interest

The authors declare no conflict of interest.

Keywords

advanced electrolytes, interface models, liquid electrolytes, Na-ion batteries, solid electrolyte interphase, transport properties, X-ray photoelectron spectroscopy

Received: September 15, 2021
Revised: October 27, 2021
Published online: January 12, 2022

[1] F. T. Wagner, B. Lakshmanan, M. F. Mathias, *J. Phys. Chem. Lett.* **2010**, *1*, 2204.
[2] B. Dunn, H. Kamath, J.-M. Tarascon, *Science* **2011**, *334*, 928.
[3] Z. Yang, J. Zhang, M. C. W. Kintner-Meyer, X. Lu, D. Choi, J. P. Lemmon, J. Liu, *Chem. Rev.* **2011**, *111*, 3577.
[4] M. S. Whittingham, *Chem. Rev.* **2014**, *114*, 11414.
[5] T. Famprikis, P. Canepa, J. A. Dawson, M. S. Islam, C. Masquelier, *Nat. Mater.* **2019**, *18*, 1278.
[6] J.-M. Tarascon, M. Armand, *Nature* **2001**, *414*, 359.
[7] M. Armand, J.-M. Tarascon, *Nature* **2008**, *451*, 652.
[8] J. B. Goodenough, K.-S. Park, *J. Am. Chem. Soc.* **2013**, *135*, 1167.
[9] J. W. Choi, D. Aurbach, *Nat. Rev. Mater.* **2016**, *1*, 16013.
[10] A. Manthiram, X. Yu, S. Wang, *Nat. Rev. Mater.* **2017**, *2*, 16103.
[11] V. Palomares, P. Serras, I. Villaluenga, K. B. Hueso, J. Carretero-González, T. Rojo, *Energy Environ. Sci.* **2012**, *5*, 5884.
[12] M. D. Slater, D. Kim, E. Lee, C. S. Johnson, *Adv. Funct. Mater.* **2013**, *23*, 947.
[13] J. Peters, D. Buchholz, S. Passerini, M. Weil, *Energy Environ. Sci.* **2016**, *9*, 1744.
[14] C. Vaalma, D. Buchholz, M. Weil, S. Passerini, *Nat. Rev. Mater.* **2018**, *3*, 18013.
[15] J. F. Peters, A. Peña Cruz, M. Weil, *Batteries* **2019**, *5*, 10.
[16] P. G. Bruce, S. A. Freunberger, L. J. Hardwick, J.-M. Tarascon, *Nat. Mater.* **2012**, *11*, 19.
[17] L. Kong, C. Yan, J.-Q. Huang, M.-Q. Zhao, M.-M. Titirici, R. Xiang, Q. Zhang, *Energy Environ. Mater.* **2018**, *1*, 100.
[18] A. Kraytsberg, Y. Ein-Eli, *Adv. Energy Mater.* **2012**, *2*, 922.
[19] N. Nitta, F. Wu, J. T. Lee, G. Yushin, *Mater. Today* **2015**, *18*, 252.
[20] P. K. Nayak, E. M. Erickson, F. Schipper, T. R. Penki, N. Munichandraiah, P. Adelhelm, H. Sclar, F. Amalraj, B. Markovsky, D. Aurbach, *Adv. Energy Mater.* **2018**, *8*, 1702397.
[21] E. Peled, S. Menkin, *J. Electrochem. Soc.* **2017**, *164*, A1703.
[22] J. Asenbauer, T. Eisenmann, M. Kuenzel, A. Kazzazi, Z. Chen, D. Bresser, *Sustainable Energy Fuels* **2020**, *4*, 5387.
[23] E. Peled, *J. Electrochem. Soc.* **1979**, *126*, 2047.
[24] L. Liu, J. Park, X. Lin, A. M. Sastry, W. Lu, *J. Power Sources* **2014**, *268*, 482.
[25] S. L. Koch, B. J. Morgan, S. Passerini, G. Teobaldi, *J. Power Sources* **2015**, *296*, 150.
[26] D. Bedrov, O. Borodin, J. B. Hooper, *J. Phys. Chem. C* **2017**, *121*, 16098.
[27] L. Raguette, R. Jorn, *J. Phys. Chem. C* **2018**, *122*, 3219.
[28] A. Wang, S. Kadam, H. Li, S. Shi, Y. Qi, *npj Comput. Mater.* **2018**, *4*, 1.
[29] A. Muralidharan, M. I. Chaudhari, L. R. Pratt, S. B. Rempe, *Sci. Rep.* **2018**, *8*, 10736.
[30] B. Horstmann, F. Single, A. Latz, *Curr. Opin. Electrochem.* **2019**, *13*, 61.
[31] D. Aurbach, M. L. Daroux, P. W. Faguy, E. Yeager, *J. Electrochem. Soc.* **1987**, *134*, 1611.
[32] D. Aurbach, O. (Youngman) Chusid, *J. Electrochem. Soc.* **1993**, *140*, L155.
[33] P. Novák, F. Joho, R. Imhof, J.-C. Panitz, O. Haas, *J. Power Sources* **1999**, *81–82*, 212.
[34] F. Kong, R. Kostecki, G. Nadeau, X. Song, K. Zaghib, K. Kinoshita, F. McLarnon, *J. Power Sources* **2001**, *97*, 58.
[35] L. Cabo-Fernandez, D. Bresser, F. Braga, S. Passerini, L. J. Hardwick, *Batteries Supercaps* **2019**, *2*, 168.
[36] K. Kwon, F. Kong, F. McLarnon, J. W. Evans, *J. Electrochem. Soc.* **2003**, *150*, A229.
[37] J. Lei, L. Li, R. Kostecki, R. Muller, F. McLarnon, *J. Electrochem. Soc.* **2005**, *152*, A774.
[38] Y. Matsumura, S. Wang, C. Yamaguchi, J. Mondori, H. Matsui, *J. Power Sources* **1998**, *74*, 246.
[39] I. Epelboin, M. Froment, M. Garreau, J. Thevenin, D. Warin, *J. Electrochem. Soc.* **1980**, *127*, 2100.
[40] G. Nazri, R. H. Muller, *J. Electrochem. Soc.* **1985**, *132*, 2050.
[41] E. Peled, D. Bar Tow, A. Merson, A. Gladkich, L. Burstein, D. Golodnitsky, *J. Power Sources* **2001**, *97–98*, 52.
[42] M. A. Muñoz-Márquez, M. Zarrabeitia, E. Castillo-Martínez, A. Eguía-Barrio, T. Rojo, M. Casas-Cabanas, *ACS Appl. Mater. Interfaces* **2015**, *7*, 7801.
[43] K. N. Wood, G. Teeter, *ACS Appl. Energy Mater.* **2018**, *1*, 4493.
[44] Y. Wang, X. Guo, S. Greenbaum, J. Liu, K. Amine, *Electrochem. Solid-State Lett.* **2001**, *4*, A68.
[45] S. J. Rezvani, M. Ciambezi, R. Gunnella, M. Minicucci, M. A. Muñoz, F. Nobili, M. Pasqualini, S. Passerini, C. Schreiner, A. Trapananti, A. Witkowska, A. Di Cicco, *J. Phys. Chem. C* **2016**, *120*, 4287.
[46] M. Balasubramanian, H. S. Lee, X. Sun, X. Q. Yang, A. R. Moodenbaugh, J. McBreen, D. A. Fischer, Z. Fu, *Electrochem. Solid-State Lett.* **2001**, *5*, A22.
[47] A. D. Cicco, A. Giglia, R. Gunnella, S. L. Koch, F. Mueller, F. Nobili, M. Pasqualini, S. Passerini, R. Tossici, A. Witkowska, *Adv. Energy Mater.* **2015**, *5*, 1500642.
[48] S. J. Rezvani, R. Gunnella, A. Witkowska, F. Mueller, M. Pasqualini, F. Nobili, S. Passerini, A. D. Cicco, *ACS Appl. Mater. Interfaces* **2017**, *9*, 4570.
[49] M. Á. Muñoz-Márquez, D. Saurel, J. L. Gómez-Cámer, M. Casas-Cabanas, E. Castillo-Martínez, T. Rojo, *Adv. Energy Mater.* **2017**, *7*, 1700463.
[50] H. S. Hirsh, Y. Li, D. H. S. Tan, M. Zhang, E. Zhao, Y. S. Meng, *Adv. Energy Mater.* **2020**, *10*, 2001274.
[51] G. Zampardi, F. L. Mantia, *Batteries Supercaps* **2020**, *3*, 672.
[52] J. B. Goodenough, *Energy Environ. Sci.* **2013**, *7*, 14.
[53] A. Etxebarria, S. L. Koch, O. Bondarchuk, S. Passerini, G. Teobaldi, M. Á. Muñoz-Márquez, *Adv. Energy Mater.* **2020**, *10*, 2000520.
[54] P. Peljo, H. H. Girault, *Energy Environ. Sci.* **2018**, *11*, 2306.
[55] S. Trasatti, *J. Electroanal. Chem. Interfacial Electrochem.* **1986**, *209*, 417.
[56] P. Verma, P. Maire, P. Novák, *Electrochim. Acta* **2010**, *55*, 6332.
[57] K. Xu, *Chem. Rev.* **2004**, *104*, 4303.
[58] P. Arora, R. E. White, M. Doyle, *J. Electrochem. Soc.* **1998**, *145*, 3647.
[59] M. G. S. R. Thomas, P. G. Bruce, J. B. Goodenough, *J. Electrochem. Soc.* **1985**, *132*, 1521.
[60] D. Aurbach, K. Gamolsky, B. Markovsky, G. Salitra, Y. Gofer, U. Heider, R. Oesten, M. Schmidt, *J. Electrochem. Soc.* **2000**, *147*, 1322.
[61] K. Edström, T. Gustafsson, J. O. Thomas, *Electrochim. Acta* **2004**, *50*, 397.
[62] S. J. Rezvani, R. Parmar, F. Maroni, F. Nobili, A. Di Cicco, R. Gunnella, *J. Phys. Chem. C* **2020**, *124*, 26670.
[63] S. Malmgren, K. Ciosek, M. Hahlin, T. Gustafsson, M. Gorgoi, H. Rensmo, K. Edström, *Electrochim. Acta* **2013**, *97*, 23.

[64] T. J. Lee, H. Kim, H. S. Hwang, J. Soon, J. Jung, J. H. Ryu, S. M. Oh, *J. Electrochem. Soc.* **2018**, *165*, A575.
[65] G. Zampardi, R. Trocoli, W. Schuhmann, F. L. Mantia, *Phys. Chem. Chem. Phys.* **2017**, *19*, 28381.
[66] R. Mogensen, D. Brandell, R. Younesi, *ACS Energy Lett.* **2016**, *1*, 1173.
[67] S. Komaba, W. Murata, T. Ishikawa, N. Yabuuchi, T. Ozeki, T. Nakayama, A. Ogata, K. Gotoh, K. Fujiwara, *Adv. Funct. Mater.* **2011**, *21*, 3859.
[68] V. A. Oltean, B. Philippe, S. Renault, R. Félix Duarte, H. Rensmo, D. Brandell, *Chem. Mater.* **2016**, *28*, 8742.
[69] B. Philippe, M. Valvo, F. Lindgren, H. Rensmo, K. Edström, *Chem. Mater.* **2014**, *26*, 5028.
[70] M. Zarrabeitia, M. Á. Muñoz-Márquez, F. Nobili, T. Rojo, M. Casas-Cabanas, *Batteries* **2017**, *3*, 16.
[71] F. Nobili, F. Croce, B. Scrosati, R. Marassi, *Chem. Mater.* **2001**, *13*, 1642.
[72] M. D. Levi, D. Aurbach, *J. Phys. Chem. B* **1997**, *101*, 4630.
[73] E. Barsoukov, D. H. Kim, H.-S. Lee, H. Lee, M. Yakovleva, Y. Gao, J. F. Engel, *Solid State Ionics* **2003**, *161*, 19.
[74] M. Zarrabeitia, F. Nobili, M. Á. Muñoz-Márquez, T. Rojo, M. Casas-Cabanas, *J. Power Sources* **2016**, *330*, 78.
[75] E. Barsoukov, *Impedance Spectroscopy*, (Ed: J. R. Macdonald), John Wiley & Sons, Inc., New York **2005**.
[76] M. D. Levi, G. Salitra, B. Markovsky, H. Teller, D. Aurbach, U. Heider, L. Heider, *J. Electrochem. Soc.* **1999**, *146*, 1279.
[77] Q.-C. Zhuang, X.-Y. Qiu, S.-D. Xu, Y.-H. Qiang, S.-G. Sun, *Diagnosis of Electrochemical Impedance Spectroscopy in Lithium-Ion Batteries*, IntechOpen, Croatia **2012**.
[78] B. A. Boukamp, *Solid State Ionics* **1986**, *20*, 31.
[79] Scribner Associates, "ZView for Windows", https://www.scribner.com/software/68-general-electrochemistr376-zview-for-windows/ (accessed: October 2021).
[80] M. Zarrabeitia, M. Casas-Cabanas, M. Á. Muñoz-Márquez, *Electrochim. Acta* **2021**, *372*, 137846.
[81] M. H. Han, E. Gonzalo, G. Singh, T. Rojo, *Energy Environ. Sci.* **2015**, *8*, 81.
[82] I. Hasa, D. Buchholz, S. Passerini, J. Hassoun, *ACS Appl. Mater. Interfaces* **2015**, *7*, 5206.
[83] C. Delmas, D. Carlier, M. Guignard, *Adv. Energy Mater.* **2021**, *11*, 2001201.
[84] M. Bianchini, P. Xiao, Y. Wang, G. Ceder, *Adv. Energy Mater.* **2017**, *7*, 1700514.
[85] P. Barpanda, L. Lander, S. Nishimura, A. Yamada, *Adv. Energy Mater.* **2018**, *8*, 1703055.
[86] J. Qian, C. Wu, Y. Cao, Z. Ma, Y. Huang, X. Ai, H. Yang, *Adv. Energy Mater.* **2018**, *8*, 1702619.
[87] Y. Xu, M. Zhou, Y. Lei, *Mater. Today* **2018**, *21*, 60.
[88] R. Rajagopalan, Y. Tang, C. Jia, X. Ji, H. Wang, *Energy Environ. Sci.* **2020**, *13*, 1568.
[89] E. Irisarri, A. Ponrouch, M. R. Palacin, *J. Electrochem. Soc.* **2015**, *162*, A2476.
[90] B. Xiao, T. Rojo, X. Li, *ChemSusChem* **2019**, *12*, 133.
[91] Z. V. Bobyleva, O. A. Drozhzhin, K. A. Dosaev, A. Kamiyama, S. V. Ryazantsev, S. Komaba, E. V. Antipov, *Electrochim. Acta* **2020**, *354*, 136647.
[92] B. Cao, H. Liu, B. Xu, Y. Lei, X. Chen, H. Song, *J. Mater. Chem. A* **2016**, *4*, 6472.
[93] M. M. Doeff, J. Cabana, M. Shirpour, *J. Inorg. Organomet. Polym. Mater.* **2014**, *24*, 5.
[94] S. Guo, J. Yi, Y. Sun, H. Zhou, *Energy Environ. Sci.* **2016**, *9*, 2978.
[95] K. Song, C. Liu, L. Mi, S. Chou, W. Chen, C. Shen, *Small* **2021**, *17*, 1903194.
[96] S. Wheeler, I. Capone, S. Day, C. Tang, M. Pasta, *Chem. Mater.* **2019**, *31*, 2619.
[97] S. Kuze, J. Kageura, S. Matsumoto, T. Nakayama, M. Makidera, M. Saka, T. Yamaguchi, T. Yamamoto, K. Nakane, *Development of a Sodium Ion Secondary Battery, R&D Report "SUMITOMO KAGAKU"*, Sumitomo Chemical Co. Ltd., Tsukuba Material Development Laboratory, Tsukuba, Japan **2013**.
[98] L. Wang, J. Song, R. Qiao, L. A. Wray, M. A. Hossain, Y.-D. Chuang, W. Yang, Y. Lu, D. Evans, J.-J. Lee, S. Vail, X. Zhao, M. Nishijima, S. Kakimoto, J. B. Goodenough, *J. Am. Chem. Soc.* **2015**, *137*, 2548.
[99] S. Roberts, E. Kendrick, *Nanotechnol. Sci. Appl.* **2018**, *11*, 23.
[100] A. Bauer, J. Song, S. Vail, W. Pan, J. Barker, Y. Lu, *Adv. Energy Mater.* **2018**, *8*, 1702869.
[101] L. Cailloce, A Battery Revolution in Motion, https://news.cnrs.fr/articles/a-battery-revolution-in-motion (accessed: November 2015).
[102] Tiamat Energy, "Our News", http://www.tiamat-energy.com/on-parle-de-nous/ (accessed: December 2019).
[103] S. Vail, Y. Lu, L. Wang, M. Nishijima, J. Lee, *US Patent 9742027B2*, **2017**.
[104] K. Smith, J. Treacher, D. Ledwoch, P. Adamson, E. Kendrick, *ECS Trans.* **2017**, *75*, 13.
[105] Y. Li, Y.-S. Hu, X. Qi, X. Rong, H. Li, X. Huang, L. Chen, *Energy Storage Mater.* **2016**, *5*, 191.
[106] "The first low-speed sodium-ion battery electric car came out and was hailed as a 'national car' – Industry news – News – HiNa Battery Technology Co., Ltd", https://www.hinabattery.com/en/index.php?id=47 (accessed: September 2018).
[107] Y.-S. Hu, S. Komaba, M. Forsyth, C. Johnson, T. Rojo, *Small Methods* **2019**, *3*, 1900184.
[108] "CATL Unveils, Its Latest Breakthrough Technology by Releasing Its First Generation of Sodium-ion Batteries", https://www.catl.com/en/news/665.html (accessed: July 2021).
[109] C. Bommier, X. Ji, *Small* **2018**, *14*, 1703576.
[110] H. Xie, Z. Wu, Z. Wang, N. Qin, Y. Li, Y. Cao, Z. Lu, *J. Mater. Chem. A* **2020**, *8*, 3606.
[111] J. Fondard, E. Irisarri, C. Courrèges, M. R. Palacin, A. Ponrouch, R. Dedryvère, *J. Electrochem. Soc.* **2020**, *167*, 070526.
[112] M. Dahbi, T. Nakano, N. Yabuuchi, S. Fujimura, K. Chihara, K. Kubota, J.-Y. Son, Y.-T. Cui, H. Oji, S. Komaba, *ChemElectroChem* **2016**, *3*, 1856.
[113] B. Xie, L. Wang, H. Li, H. Huo, C. Cui, B. Sun, Y. Ma, J. Wang, G. Yin, P. Zuo, *Energy Storage Mater.* **2021**, *36*, 99.
[114] R. I. R. Blyth, H. Buqa, F. P. Netzer, M. G. Ramsey, J. O. Besenhard, P. Golob, M. Winter, *Appl. Surf. Sci.* **2000**, *167*, 99.
[115] Y. Xie, P. M. A. Sherwood, *Chem. Mater.* **1990**, *2*, 293.
[116] S. Bhattacharyya, C. Cardinaud, G. Turban, *J. Appl. Phys.* **1998**, *83*, 4491.
[117] S. Bhattacharyya, J. Hong, G. Turban, *J. Appl. Phys.* **1998**, *83*, 3917.
[118] M. Dahbi, T. Nakano, N. Yabuuchi, T. Ishikawa, K. Kubota, M. Fukunishi, S. Shibahara, J.-Y. Son, Y.-T. Cui, H. Oji, S. Komaba, *Electrochem. Commun.* **2014**, *44*, 66.
[119] G. G. Eshetu, T. Diemant, M. Hekmatfar, S. Grugeon, R. J. Behm, S. Laruelle, M. Armand, S. Passerini, *Nano Energy* **2019**, *55*, 327.
[120] H. Kim, F. Wu, J. T. Lee, N. Nitta, H.-T. Lin, M. Oschatz, W. I. Cho, S. Kaskel, O. Borodin, G. Yushin, *Adv. Energy Mater.* **2015**, *5*, 1401792.
[121] S. Doubaji, B. Philippe, I. Saadoune, M. Gorgoi, T. Gustafsson, A. Solhy, M. Valvo, H. Rensmo, K. Edström, *ChemSusChem* **2016**, *9*, 97.
[122] M. Dahbi, M. Fukunishi, T. Horiba, N. Yabuuchi, S. Yasuno, S. Komaba, *J. Power Sources* **2017**, *363*, 404.
[123] C. D. Wagner, W. M. Riggs, L. E. Davis, J. F. Moulder, G. E. Muilenberg, *Handbook of X-Ray Photoelectron Spectroscopy*, Perkin-Elmer Corporation, Physical Electronics Division, Eden Prairie, Minnesota, USA **1979**.

[124] L. Baggetto, E. Allcorn, A. Manthiram, G. M. Veith, *Electrochem. Commun.* **2013**, *27*, 168.
[125] L. Baggetto, P. Ganesh, R. P. Meisner, R. R. Unocic, J.-C. Jumas, C. A. Bridges, G. M. Veith, *J. Power Sources* **2013**, *234*, 48.
[126] L. Bodenes, A. Darwiche, L. Monconduit, H. Martinez, *J. Power Sources* **2015**, *273*, 14.
[127] L. Ji, M. Gu, Y. Shao, X. Li, M. H. Engelhard, B. W. Arey, W. Wang, Z. Nie, J. Xiao, C. Wang, J.-G. Zhang, J. Liu, *Adv. Mater.* **2014**, *26*, 2901.
[128] Z. Lin, Q. Xia, W. Wang, W. Li, S. Chou, *InfoMat* **2019**, *1*, 376.
[129] C. Geng, D. Buchholz, G.-T. Kim, D. V. Carvalho, H. Zhang, L. G. Chagas, S. Passerini, *Small Methods* **2019**, *3*, 1800208.
[130] S. Komaba, T. Ishikawa, N. Yabuuchi, W. Murata, A. Ito, Y. Ohsawa, *ACS Appl. Mater. Interfaces* **2011**, *3*, 4165.
[131] G. H. Wrodnigg, J. O. Besenhard, M. Winter, *J. Electrochem. Soc.* **1999**, *146*, 470.
[132] M. Kobayashi, T. Inoguchi, T. Iida, T. Tanioka, H. Kumase, Y. Fukai, *J. Fluorine Chem.* **2003**, *120*, 105.
[133] G. G. Eshetu, M. Martinez-Ibañez, E. Sánchez-Diez, I. Gracia, C. Li, L. M. Rodriguez-Martinez, T. Rojo, H. Zhang, M. Armand, *Chem. – Asian J.* **2018**, *13*, 2770.
[134] M. M. Doeff, Y. Ma, S. J. Visco, L. C. D. Jonghe, *J. Electrochem. Soc.* **1993**, *140*, L169.
[135] D. A. Stevens, J. R. Dahn, *J. Electrochem. Soc.* **2000**, *147*, 1271.
[136] C. Bommier, D. Leonard, Z. Jian, W. F. Stickle, P. A. Greaney, X. Ji, *Adv. Mater. Interfaces* **2016**, *3*, 1600449.
[137] H. Moon, M. Zarrabeitia, E. Frank, O. Böse, M. Enterría, D. Saurel, I. Hasa, S. Passerini, *Batteries Supercaps* **2021**, *4*, 960.
[138] A. Ponrouch, A. R. Goñi, M. R. Palacín, *Electrochem. Commun.* **2013**, *27*, 85.
[139] M. Carboni, J. Manzi, A. R. Armstrong, J. Billaud, S. Brutti, R. Younesi, *ChemElectroChem* **2019**, *6*, 1745.
[140] J. W. Wang, X. H. Liu, S. X. Mao, J. Y. Huang, *Nano Lett.* **2012**, *12*, 5897.
[141] L. Xiao, Y. Cao, J. Xiao, W. Wang, L. Kovarik, Z. Nie, J. Liu, *Chem. Commun.* **2012**, *48*, 3321.
[142] S. Komaba, Y. Matsuura, T. Ishikawa, N. Yabuuchi, W. Murata, S. Kuze, *Electrochem. Commun.* **2012**, *21*, 65.
[143] W. Li, T. Liu, J. Zhang, N. Peng, R. Zheng, H. Yu, Y. Bai, Y. Cui, J. Shu, *Sustainable Energy Fuels* **2019**, *3*, 2668.
[144] I. Mohammad, L. Blondeau, E. Foy, J. Leroy, E. Leroy, H. Khodja, M. Gauthier, *Sustainable Energy Fuels* **2021**, *5*, 3825.
[145] N. Yabuuchi, Y. Matsuura, T. Ishikawa, S. Kuze, J.-Y. Son, Y.-T. Cui, H. Oji, S. Komaba, *ChemElectroChem* **2014**, *1*, 580.
[146] J. Qian, X. Wu, Y. Cao, X. Ai, H. Yang, *Angew. Chem., Int. Ed.* **2013**, *52*, 4633.
[147] P. Senguttuvan, G. Rousse, V. Seznec, J.-M. Tarascon, M. R. Palacín, *Chem. Mater.* **2011**, *23*, 4109.
[148] M. Zarrabeitia, E. Castillo-Martínez, J. M. López Del Amo, A. Eguía-Barrio, M. Á. Muñoz-Márquez, T. Rojo, M. Casas-Cabanas, *Acta Mater.* **2016**, *104*, 125.
[149] H. Pan, X. Lu, X. Yu, Y.-S. Hu, H. Li, X.-Q. Yang, L. Chen, *Adv. Energy Mater.* **2013**, *3*, 1186.
[150] S. Tanuma, C. J. Powell, D. R. Penn, *Surf. Interface Anal.* **2011**, *43*, 689.
[151] J. B. Goodenough, Y. Kim, *Chem. Mater.* **2010**, *22*, 587.
[152] Y. You, A. Manthiram, *Adv. Energy Mater.* **2018**, *8*, 1701785.
[153] C. Fang, Y. Huang, W. Zhang, J. Han, Z. Deng, Y. Cao, H. Yang, *Adv. Energy Mater.* **2016**, *6*, 1501727.
[154] K. Hurlbutt, S. Wheeler, I. Capone, M. Pasta, *Joule* **2018**, *2*, 1950.
[155] B. Xie, Y. Du, Y. Ma, S. Liu, Y. Wang, P. Zuo, Y. Gao, G. Yin, *ACS Sustainable Chem. Eng.* **2021**, *9*, 5809.
[156] W. Ren, M. Qin, Z. Zhu, M. Yan, Q. Li, L. Zhang, D. Liu, L. Mai, *Nano Lett.* **2017**, *17*, 4713.
[157] H. Fu, M. Xia, R. Qi, X. Liang, M. Zhao, Z. Zhang, X. Lu, G. Cao, *J. Power Sources* **2018**, *399*, 42.
[158] M. H. Lee, S. J. Kim, D. Chang, J. Kim, S. Moon, K. Oh, K.-Y. Park, W. M. Seong, H. Park, G. Kwon, B. Lee, K. Kang, *Mater. Today* **2019**, *29*, 26.
[159] L. A. Ma, A. J. Naylor, L. Nyholm, R. Younesi, *Angew. Chem., Int. Ed.* **2021**, *60*, 4855.
[160] M. Nose, H. Nakayama, K. Nobuhara, H. Yamaguchi, S. Nakanishi, H. Iba, *J. Power Sources* **2013**, *234*, 175.
[161] Y. Uebou, T. Kiyabu, S. Okada, J.-I. Yamaki, *Rep. Inst. Adv. Mater. Study, Kyushu Univ.* **2002**, *16*, 1.
[162] S. Y. Lim, H. Kim, R. A. Shakoor, Y. Jung, J. W. Choi, *J. Electrochem. Soc.* **2012**, *159*, A1393.
[163] K. Saravanan, C. W. Mason, A. Rudola, K. H. Wong, P. Balaya, *Adv. Energy Mater.* **2013**, *3*, 444.
[164] R. Klee, M. J. Aragón, P. Lavela, R. Alcántara, J. L. Tirado, *ACS Appl. Mater. Interfaces* **2016**, *8*, 23151.
[165] H. Zhang, I. Hasa, B. Qin, T. Diemant, D. Buchholz, R. J. Behm, S. Passerini, *ChemElectroChem* **2017**, *4*, 1256.
[166] S. Mariyappan, Q. Wang, J.-M. Tarascon, *J. Electrochem. Soc.* **2018**, *165*, A3714.
[167] M. Zarrabeitia, E. Gonzalo, M. Pasqualini, M. Ciambezi, O. Lakuntza, F. Nobili, A. Trapananti, A. D. Cicco, G. Aquilanti, N. A. Katcho, J. M. L. del Amo, J. Carrasco, M. Á. Muñoz-Márquez, T. Rojo, *J. Mater. Chem. A* **2019**, *7*, 14169.
[168] J. Hwang, K. Matsumoto, R. Hagiwara, *Adv. Energy Mater.* **2020**, *10*, 2001880.
[169] G. Yan, R. Dugas, J.-M. Tarascon, *J. Electrochem. Soc.* **2018**, *165*, A220.
[170] K. Subramanyan, Y.-S. Lee, V. Aravindan, *J. Colloid Interface Sci.* **2021**, *582*, 51.
[171] K. Kubota, N. Yabuuchi, H. Yoshida, M. Dahbi, S. Komaba, *MRS Bull.* **2014**, *39*, 416.
[172] C. Delmas, C. Fouassier, P. Hagenmuller, *Physica B+C* **1980**, *99*, 81.
[173] J.-Y. Hwang, S.-M. Oh, S.-T. Myung, K. Y. Chung, I. Belharouak, Y.-K. Sun, *Nat. Commun.* **2015**, *6*, 6865.
[174] J. Song, K. Wang, J. Zheng, M. H. Engelhard, B. Xiao, E. Hu, Z. Zhu, C. Wang, M. Sui, Y. Lin, D. Reed, V. L. Sprenkle, P. Yan, X. Li, *ACS Energy Lett.* **2020**, *5*, 1718.
[175] S. Guo, Q. Li, P. Liu, M. Chen, H. Zhou, *Nat. Commun.* **2017**, *8*, 135.
[176] M. Zarrabeitia, L. Gomes Chagas, M. Kuenzel, E. Gonzalo, T. Rojo, S. Passerini, M. Á. Muñoz-Márquez, *ACS Appl. Mater. Interfaces* **2019**, *11*, 28885.
[177] A. J. Fernández-Ropero, M. Zarrabeitia, G. Baraldi, M. Echeverria, T. Rojo, M. Armand, D. Shanmukaraj, *ACS Appl. Mater. Interfaces* **2021**, *13*, 11814.
[178] W. Zhou, M. Zhang, X. Kong, W. Huang, Q. Zhang, *Adv. Sci.* **2021**, *8*, 2004490.
[179] Y. Wang, S. Song, C. Xu, N. Hu, J. Molenda, L. Lu, *Nano Mater. Sci.* **2019**, *1*, 91.
[180] J. Zheng, Y. Yang, W. Li, X. Feng, W. Chen, Y. Zhao, *J. Mater. Chem. A* **2020**, *8*, 22962.
[181] F. Gebert, J. Knott, R. Gorkin, S.-L. Chou, S.-X. Dou, *Energy Storage Mater.* **2021**, *36*, 10.
[182] A. Basile, M. Hilder, F. Makhlooghiazad, C. Pozo-Gonzalo, D. R. MacFarlane, P. C. Howlett, M. Forsyth, *Adv. Energy Mater.* **2018**, *8*, 1703491.
[183] K. Xu, *Chem. Rev.* **2014**, *114*, 11503.
[184] M. Lee, J. Hong, J. Lopez, Y. Sun, D. Feng, K. Lim, W. C. Chueh, M. F. Toney, Y. Cui, Z. Bao, *Nat. Energy* **2017**, *2*, 861.
[185] X. Liu, B. Qin, H. Zhang, A. Moretti, S. Passerini, *ACS Appl. Energy Mater.* **2019**, *2*, 2786.
[186] B. Jache, P. Adelhelm, *Angew. Chem., Int. Ed.* **2014**, *53*, 10169.
[187] P. Walden, *Bull. Acad. Imp. Sci. St. -Pétersbourg* **1914**, *8*, 405.

[188] K. Matsumoto, T. Hosokawa, T. Nohira, R. Hagiwara, A. Fukunaga, K. Numata, E. Itani, S. Sakai, K. Nitta, S. Inazawa, *J. Power Sources* **2014**, *265*, 36.
[189] J. Serra Moreno, G. Maresca, S. Panero, B. Scrosati, G. B. Appetecchi, *Electrochem. Commun.* **2014**, *43*, 1.
[190] C.-H. Wang, C.-H. Yang, J.-K. Chang, *Chem. Commun.* **2016**, *52*, 10890.
[191] H. Usui, Y. Domi, K. Fujiwara, M. Shimizu, T. Yamamoto, T. Nohira, R. Hagiwara, H. Sakaguchi, *ACS Energy Lett.* **2017**, *2*, 1139.
[192] C. V. Manohar, T. C. Mendes, M. Kar, D. Wang, C. Xiao, M. Forsyth, S. Mitra, D. R. MacFarlane, *Chem. Commun.* **2018**, *54*, 3500.
[193] L. G. Chagas, S. Jeong, I. Hasa, S. Passerini, *ACS Appl. Mater. Interfaces* **2019**, *11*, 22278.
[194] Y.-E. Zhu, L. Yang, X. Zhou, F. Li, J. Wei, Z. Zhou, *J. Mater. Chem. A* **2017**, *5*, 9528.
[195] P. Bai, Y. He, P. Xiong, X. Zhao, K. Xu, Y. Xu, *Energy Storage Mater.* **2018**, *13*, 274.
[196] A. Fukunaga, T. Nohira, R. Hagiwara, K. Numata, E. Itani, S. Sakai, K. Nitta, S. Inazawa, *J. Power Sources* **2014**, *246*, 387.
[197] M. C. Kroon, W. Buijs, C. J. Peters, G.-J. Witkamp, *Green Chem.* **2006**, *8*, 241.
[198] H. Usui, Y. Domi, N. Takada, H. Sakaguchi, *Cryst. Growth Des.* **2021**, *21*, 218.
[199] C. Ding, T. Nohira, R. Hagiwara, *J. Power Sources* **2017**, *354*, 10.
[200] T. Shiga, H. Kondo, Y. Kato, M. Inoue, *J. Phys. Chem. C* **2015**, *119*, 27946.
[201] Z. Liu, G. Pulletikurthi, F. Endres, *ACS Appl. Mater. Interfaces* **2016**, *8*, 12158.
[202] K. Westman, R. Dugas, P. Jankowski, W. Wieczorek, G. Gachot, M. Morcrette, E. Irisarri, A. Ponrouch, M. R. Palacín, J.-M. Tarascon, P. Johansson, *ACS Appl. Energy Mater.* **2018**, *1*, 2671.
[203] F. Wu, N. Zhu, Y. Bai, Y. Li, Z. Wang, Q. Ni, H. Wang, C. Wu, *Nano Energy* **2018**, *51*, 524.
[204] C.-Y. Chen, T. Kiko, T. Hosokawa, K. Matsumoto, T. Nohira, R. Hagiwara, *J. Power Sources* **2016**, *332*, 51.
[205] M. Okoshi, Y. Yamada, A. Yamada, H. Nakai, *J. Electrochem. Soc.* **2013**, *160*, A2160.
[206] F. Makhlooghiazad, M. Sharma, Z. Zhang, P. C. Howlett, M. Forsyth, L. F. Nazar, *J. Phys. Chem. Lett.* **2020**, *11*, 2092.
[207] I. Hasa, X. Dou, D. Buchholz, Y. Shao-Horn, J. Hassoun, S. Passerini, B. Scrosati, *J. Power Sources* **2016**, *310*, 26.
[208] L. G. Chagas, D. Buchholz, L. Wu, B. Vortmann, S. Passerini, *J. Power Sources* **2014**, *247*, 377.
[209] X. Cheng, R. Zhang, C. Zhao, F. Wei, J. Zhang, Q. Zhang, *Adv. Sci.* **2015**, *3*, 1500213.
[210] J. G. Thevenin, R. H. Muller, *J. Electrochem. Soc.* **1987**, *134*, 273.

Miguel Ángel Muñoz-Márquez is an Associate Professor of Physical Chemistry at the University of Camerino (Italy). Until October 2021, he was the group leader responsible for surface and interface analysis at CIC energiGUNE (Spain). He obtained his Ph.D. in Physics from the University of Warwick (United Kingdom) in 2005. His research interests lie in the experimental investigation of surface and interface phenomena of energy storage systems with special emphasis on the physicochemical aspects of battery interfaces. Since 2019, Miguel Ángel is a member of the Governing Board of the Specialized Group in Energy at the Spanish Royal Physics Society.

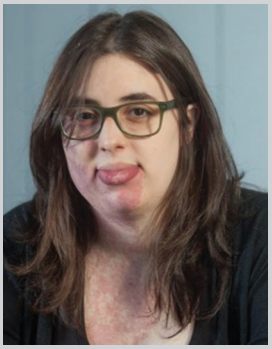

Maider Zarrabeitia joined the group of Prof. Stefano Passerini at Helmholtz-Institute Ulm (HIU) in 2018 as a visitor researcher. Currently she is leading the sodium-ion battery group at HIU focusing on electrode materials and electrolytes for sodium-ion batteries as well as understanding the electrode-electrolyte interphases for several battery technologies such as Li-ion, Li-metal, and Na-ion. Maider received her Ph.D. in Materials Science and Technology in 2016 from the University of Basque Country (UPV/EHU, Spain) while being a researcher of CIC energiGUNE in the group of Dr. Miguel Ángel Muñoz, including two research stages at the University of Camerino (Italy).

Stefano Passerini is a Professor at Karlsruhe Institute of Technology and Director of Helmholtz Institute Ulm. His research focuses on the basic understanding and development of materials for high-energy batteries with the goal to develop sustainable energy storage systems. Co-author of >600 scientific papers (Scopus H-Index: 96), a few book chapters, and several international patents, he has been awarded in 2012 the Research Award of the Electrochemical Society Battery Division. He has been nominated Fellow of the International Society of Electrochemistry (2016) and the Electrochemical Society (2020). Since 2019, he is a member of the Leopoldina Academy of Science.

Teófilo Rojo became a full Professor of Inorganic Chemistry at the University of the Basque Country(UPV/EHU) in 1992. His research has been focused on Solid State Chemistry and Materials Science. From 2010 to 2020 he was the Scientific Director of the CIC energiGUNE developing materials for advanced batteries (lithium, sodium, redox, etc.). In 2015 he was appointed as a Correspondent Academic Member of the Royal Spanish Academy of Exacts, Physical and Natural Sciences, and in 2016 he was named a member of the Working Party on Chemistry and Energy of EuCheMS (European Chemical Science).